Pharm Res (2013) 30:761–780
DOI 10.1007/s11095-012-0918-y

RESEARCH PAPER

Cyclosporine Inhibition of Hepatic and Intestinal CYP3A4, Uptake and Efflux Transporters: Application of PBPK Modeling in the Assessment of Drug-Drug Interaction Potential

Michael Gertz • Catherine M. Cartwright • Michael J. Hobbs • Kathryn E. Kenworthy • Malcolm Rowland • J. Brian Houston • Aleksandra Galetin

Received: 29 August 2012 / Accepted: 15 October 2012 / Published online: 22 November 2012

ABSTRACT

Purpose To apply physiologically-based pharmacokinetic (PBPK) modeling to investigate the consequences of reduction in activity of hepatic and intestinal uptake and efflux transporters by cyclosporine and its metabolite AM1.

Methods Inhibitory potencies of cyclosporine and AM1 against OATP1B1, OATP1B3 and OATP2B1 were investigated in HEK293 cells +/− pre-incubation. Cyclosporine PBPK model implemented in Matlab was used to assess interaction potential (+/− metabolite) against different processes (uptake, efflux and metabolism) in liver and intestine and to predict quantitatively drug-drug interaction with repaglinide.

Results Cyclosporine and AM1 were potent inhibitors of OATP1B1 and OATP1B3, IC_{50} ranging from 0.019–0.093 μM following pre-incubation. Cyclosporine PBPK model predicted the highest interaction potential against liver uptake transporters, with a maximal reduction of >70% in OATP1B1 activity; the effect on hepatic efflux and metabolism was minimal. In contrast, 80–97% of intestinal P-gp and CYP3A4 activity was reduced due to the 50-fold higher cyclosporine enterocytic concentrations relative to unbound hepatic inlet. The inclusion of AM1 resulted in a minor increase in the predicted maximal reduction of OATP1B1/1B3 activity. Good predictability of cyclosporine-repaglinide DDI and the impact of dose staggering are illustrated.

Conclusions This study highlights the application of PBPK modeling for quantitative prediction of transporter-mediated DDIs with concomitant consideration of P450 inhibition.

KEY WORDS cyclosporine · drug-drug interactions · OATP1B1 · OATP1B3 · physiologically-based pharmacokinetic models

ABBREVIATIONS

AM1	mono-hydroxylated metabolite of cyclosporine A (Hawk's nomenclature)
CsA	cyclosporine A
CYP enzymes	Cytochrome P450 enzymes
DDI(s)	drug-drug interaction(s)
HEK-cells	human embryonic kidney cells
IC_{50}	inhibitory constant (concentration at which 50% of total inhibitory effect is observed)
IVIVE	*in vitro-in vivo* extrapolation
OATP	organic anion transporter proteins
PBPK model	physiologically-based pharmacokinetic model

INTRODUCTION

Investigation of potential transporter mediated drug-drug interactions (DDI) is becoming increasingly important considering the large number of drugs reported to be either substrates or inhibitors of active hepatic uptake processes.

Electronic supplementary material The online version of this article (doi:10.1007/s11095-012-0918-y) contains supplementary material, which is available to authorized users.

M. Gertz • M. Rowland • J. B. Houston • A. Galetin (✉)
Centre for Applied Pharmacokinetic Research
School of Pharmacy and Pharmaceutical Sciences
University of Manchester
Oxford Road
M13 9PT Manchester, UK
e-mail: Aleksandra.Galetin@manchester.ac.uk

C. M. Cartwright • M. J. Hobbs • K. E. Kenworthy
Department of Drug Metabolism and Pharmacokinetics
GlaxoSmithKline
Ware, UK

Simple static prediction models based on ratios of inhibitor concentration and its potency (I/K_i) have been applied for the prediction of transporter-mediated DDIs (1–4). However, these approaches ignore the potential effect of multiple transporters, transporter-enzyme interplay in different tissues and the role of passive diffusion. Efforts have been made to address contribution of multiple uptake transporters to the victim drug disposition by introducing the parameter fraction of drug transported (f_T) in the static transporter DDI model (1) (analogous to fraction metabolized) and to investigate multiple interaction mechanisms (4). However, these approaches do not accommodate the dynamic nature of the processes mentioned above and concentration of the inhibitor is assumed to be constant, as a reflection of the 'worst case scenario'.

The largest proportion of reported transporter-mediated DDIs involve interactions with cyclosporine A (CsA) (Table I), a potent inhibitor of a number of uptake and efflux transporters *in vitro*. For several of these DDIs, hepatic uptake is believed to contribute rather than being the sole determinant of the DDI observed, as apparent in the cases of atorvastatin, lovastatin, simvastatin and rosuvastatin. Some of these victim drugs show multiple transporter specificities, e.g., rosuvastatin is a substrate for a number of uptake and efflux transporters (5–7) or may involve different sites for the interaction (e.g., lovastatin and simvastatin are metabolized extensively both in the liver and intestine). One major confounding factor in the interpretation of CsA clinical data is the common practice of reporting the magnitude of DDI in individuals receiving chronic CsA dosing after organ transplantation in comparison to historic data in healthy volunteers; exceptions are clinical studies with atorvastatin, repaglinide and simvastatin where the pharmacokinetics of the victim drug was assessed in the same individuals before and after CsA administration (Table I). Furthermore, it is evident from the large body of literature that CsA is a rather non-specific inhibitor with substantial potency against various transport and metabolic processes. Also, large inter-laboratory variability in inhibition data is apparent even for data obtained in the same cellular system, as summarized in Supplementary Material, Table SI.

CsA has three primary metabolites AM1, AM9 and AM4N (8). Of these metabolites, AM1 reaches the highest blood concentrations which have been reported to exceed those of CsA after single and/or multiple drug administration (9–12). Additionally, AM9 reaches appreciable blood levels, while AM4N and the secondary metabolites (AM1c and AM19) attain considerably lower blood concentrations in comparison to CsA (10,13–15).

Table I Reported Drug-Drug Interactions with CsA as Inhibitor

	AUC_I/ AUC[a]	$Cmax_I$/ Cmax	SLCO1B1 polymorphic study	Comments
Atorvastatin	7.4	6.6	Yes	A
	8.7	10.7		A
	15.3	13.7		B
Bosentan	3.3	2.3	n/a	A, C
Cerivastatin	3.7	3.4–5.0	n/a	A, D
Fluvastatin	3.3	4.1–6.0	Yes[c]	A, D
Lovastatin	17.6	>20	n/a	A, D
Pravastatin[b]	5.5	2.9	Yes	A
	11.8	7.0		A
Repaglinide	2.4	1.75	Yes	B
Rosuvastatin	4.8–8.3	6.9–12.2	Yes	A, E
Simvastatin	8.0	7.6	Yes[d]	B

n/a, not available

[a] all references are listed in the Supplementary material (Table SXII)

[b] Additional and comparable data have been reported in children (65)

[c] Fluvastatin AUC not significantly different between SCLO1B1 genotypes (66)

[d] Significant effect on simvastatin acid AUC, no effect on simvastatin lactone AUC (67); A, AUC increase was assessed in comparison to historic data and not in a cross-over study design; B, AUC increase was assessed in the same individuals; C, bosentan is an inducer of its own metabolism and CsA interaction data reported in Binet *et al*. (2000) were therefore compared to bosentan AUC at stead-state for the same dose regimen reported elsewhere (68); D, average fold-change of single dose and steady-state data; E, multiple dose levels (10 and 20 mg) and dose regimens (single dose and steady-state) were available for rosuvastatin

Currently, no data exist to indicate whether these metabolites may contribute to the clinical DDIs observed. This issue is of particular relevance considering recent FDA recommendation to assess the role of metabolites when their exposure exceeds 25% of the parent (16).

The current study aimed to investigate the interaction potential of CsA in two complementary ways. Initially, *in vitro* inhibitory potency data were determined for the key hepatic uptake transporters (OATP1B1, OATP1B3 and OATP2B1) in order to elucidate the apparently increased potency of CsA after pre-incubation reported for OATP1B1 (17). In addition, inhibition potency of CsA's main metabolite AM1 was investigated against the same transporters using the same experimental design as for CsA. The second part of the current study aimed to assess CsA concentrations and DDI potential at the two relevant sites (liver and enterocytes) using a physiologically-based pharmacokinetic (PBPK) model. The CsA PBPK model was constructed based on tissue and blood distribution data

reported in rat or human (18–21) in conjunction with human physiology data (detailed list in Supplementary Material Table SII). The oral PBPK model included a compartmental absorption and transit model (22,23) to allow a mechanistic description of CsA enterocytic concentration and assessment of interactions at the level of the intestine. Initial PBPK model optimization and validation was performed across different CsA formulations and routes of administration (i.v. and oral Sandimmune® and Neoral®). Finally, the *in vitro* information on CsA potency and the appropriate concentration-time profiles generated within the CsA PBPK model were utilized to predict the time course of the interaction potential of CsA on a range of uptake and efflux transporters (OATP1B1, OATP1B3, NTCP, P-gp, MRP2, BSEP and BCRP) and CYP3A both at the level of the liver and small intestine. In addition, a mechanistic assessment of the reduction in transporter/enzyme activity over CsA dosing interval was performed by including the contribution of AM1 metabolite. The predictive capabilities of the current PBPK model are illustrated using the example of the CsA-repaglinide DDI; the latter being reported to be a substrate for hepatic uptake transporters and CYP3A4/CYP2C8 (24,25).

The current work provides a mechanistic framework for future quantitative prediction of CsA interactions with new chemical entities which display active hepatic uptake, intestinal metabolism and efflux. In addition, the repaglinide example illustrates clearly the application of PBPK modeling to guide the design of clinical studies and its value in modifying dosage regimens in order to avoid possible DDIs.

MATERIAL AND METHODS

Reagents

Cyclosporine A (Sigma Aldrich, UK), [^{3}H]-cyclosporine A (Perkin Elmer, US), AM1 (Toronto Research Chemicals Inc, Canada), [^{3}H]-estradiol 17β-D-glucuronide (Perkin Elmer, US and Quotient, UK), [^{3}H]-estrone sulfate, ammonium salt (Perkin Elmer, US), rifamycin SV™ (Sigma Aldrich, UK), human embryonic kidney MSRII cell line (HEK), transduced with BacMam baculovirus containing the human organic anion transporting polypeptide 1B1, 1B3 or 2B1 (OATP1B1, OATP1B3 or OATP2B1) were used (GlaxoSmithKline, UK). 24-well assay plates (BD Biosciences, UK), Dulbecco's modified Eagle's medium F12 containing 10% foetal bovine serum (Gilco, UK), Geneticin (Gibco, UK), sodium butyrate (Sigma, UK), Dulbecco's Phosphate Buffered Saline (DPBS) (Invitrogen, UK) and dimethyl sulphoxide (Sigma, UK).

A systematic search for any reports on CsA potency against main uptake transporters, efflux transporters and metabolic enzymes was undertaken. The main transporter/enzymes for which IC_{50} (or K_i) data were available included the uptake transporters: NTCP, OATP1B1, OATP1B3 and OATP2B1; the efflux transporters: BCRP, BSEP, P-gp, MRP2 and the metabolic enzyme: CYP3A4. The search included hits for any of the different pseudonyms of the transporters OATP1B1 (OATP-C, LST-1, OATP2), OATP1B3 (OATP8), OATP2B1 (OATP-B), BSEP (BAT, SPGP), MRP2 (cMOAT), BCRP (MXR) and cyclosporine (cyclosporin, ciclosporin). In addition to searches in Pubmed, the online databases TP-search (http://125.206.112.67/tp-search/login.php) and UCSF-FDA TransPortal (http://bts.ucsf.edu/fdatransportal/#content) were sourced. The cell or subcellular systems considered in this study included membrane vesicles, HEK cells, Caco-2 cells, LLC-PK1 cells, MDCK cells, HeLa cells and human liver microsomes. A complete list of CsA IC_{50} or K_i values against a range of transporters and CYP3A4 is provided in Supplementary Material, Table SI. Despite relatively high availability of IC_{50} data for some of the uptake and efflux transporters in the literature, there is an uncertainty associated with the quality of some of the reports which may bias subsequent assessment of CsA interaction potential. In particular, available literature data posed the question of whether reported CsA IC_{50} estimates have been biased because of binding, as a number of previous studies exceeded aqueous solubility of CsA (by up to 20-fold) without this being apparent in the IC_{50} plots (5,26–28).

Clinical DDI studies with CsA as an inhibitor were also collated from the literature; changes in the AUC and C_{max} as a result of CsA co-administration are summarized in Table I. In the cases when the control and inhibitor phase of the study were not performed in the same population attempts were made to match the age and dose of the historic data to the actual interaction study. Information on the impact of other covariates e.g., disease or co-medication were not available which may contribute to the observed interaction possibly leading to bias when assessing an AUC ratio based on comparison to healthy individuals.

Determination of *In Vitro* IC_{50} Values of CsA and AM1

The current study assessed the IC_{50} values of CsA and AM1 against OATP1B1, OATP1B3 and OATP2B1 in transiently transfected HEK-293 cells. The methodology has been described in detail elsewhere (1). The CsA and AM1 concentrations assessed were 0, 3, 15, 30, 60, 150, 300, 600, 1500, 3000 and 6000 nM (upper limit represents the solu-

bility of CsA in aqueous media (29,30)). Experiments were performed in duplicates on at least three separate occasions. The probe substrates used were [^{3}H]-estradiol glucuronide for OATP1B1 and OATP1B3 (0.02 to 0.06 μM) or [^{3}H]-estrone sulfate for OATP2B1 (0.02 μM). Low probe substrate concentrations ([S]<<K_m) were used to ensure unbiased parameter estimates regardless of the transporter inhibition mechanism (competitive or noncompetitive inhibition of the transporter), i.e., that IC_{50}=K_i. Cellular uptake of the probe substrate was assessed for 0.5, 3 or 10 min for OATP2B1, OATP1B1 and OATP1B3, respectively. Rifamycin was used as control inhibitor in all assays either at 10 μM for OATP1B1 and OATP1B3 or 100 μM for OATP2B1. After incubation, the working solution was removed from each well and the experiment stopped by washing three times with 800 μL cold (4°C) DPBS prior to solubilization with 400 μL of 1% (v/v) Triton X-100. Aliquots of 100 μL of each well were transferred into a 96-well Lumaplate. The plates were left overnight in a drying cabinet and analyzed for total radioactivity using a microplate scintillation and luminescence counter, Topcount NXT (Perkin Elmer, UK).

The cellular uptake rates of the probe substrate were determined in the presence of increasing concentrations of CsA and AM1 before and after pre-incubation of 30–45 min; the impact of pre-incubation on CsA and AM1 potency was assessed for all three transporters investigated. The IC_{50} estimates were obtained in R v.2.15 (The R Foundation for Statistical Computing) by fitting Eq. 1 to the data (22 data points per experiment) using a nonlinear least squares fitting routine. Criteria to include experiments for analysis were a signal-to-noise ratio of greater than 3 (quotient of $CLint_{uptake}$ in the absence and presence of rifamycin) and standard errors on IC_{50} values of less than 40%.

$$CLint_{uptake} = \frac{CLint_{range}}{1 + ([I]/IC_{50})^{s}} + B \quad (1)$$

where $CLint_{uptake}$ represents the intrinsic uptake clearance at inhibitor concentration [I] (μL/(cm^2.min)); $CLint_{range}$, the range of intrinsic uptake clearances; s, the slope factor and B, the background velocity.

PBPK Modeling of CsA in Human After Intravenous Dosing

A PBPK model of CsA in human was constructed in analogy to previously published data in rat (19,20) using physiological parameters reported for standard male (detailed list in Supplementary Material Table SII). The rate equations of the PBPK model were implemented in Matlab v.7.12 (The MathWorks, Inc.). The rate equations for the liver model are outlined below and refer to total and unbound concentrations (C and Cu, respectively) in red blood cells residing in the tissue (Eqs. 2 and 3, respectively), extracellular concentration (Eq. 4), non-saturable (Eq. 5) and saturable intracellular (Eq. 6) compartments.

A complete summary of all the parameters used in the CsA PBPK model is provided in the Supplementary Material (Tables SIII–VI) together with the rate equations describing the different local tissue models. In short, the current model describes the distribution and metabolism of CsA in 10 tissues (adipose, muscle, lung, heart, bone, skin, kidney, liver intestine and brain); unaccounted body volume and blood flow were small (approx. 5%) and were added to the muscle compartment. Parameters describing tissue distribution were taken from the rat under the assumption of equality between species in the following parameters—fu_T, K_{ass} (association constant), Bt_T (total binding sites), K_D (binding affinity constant), k_{on} and k_{off} (on- and off-rates). Summary of parameters obtained in rats is provided in Supplementary Material Table SIII. PS_{TC} values, the product of drug permeability and tissue surface area, were scaled from rat to human using allometry (PS_{TC}= $A.V^{0.75}$) whereas PS_{BC} expressed as L/h per L of blood was scaled by blood volume. Other parameters were sourced from the literature for human e.g., fu_p, nP_T (number of binding sites in red blood cells), $K_{D,BC}$ (binding affinity constant in red blood cells), as summarized in Supplementary Material Table SIV. As the fraction unbound used in the current analysis differed (3 *vs.* 6%) from the fu_p in the original study which estimated nP_T and $K_{D,BC}$ (31) these parameters were refitted using the current fu_p value in order to recover the relationship between total plasma concentration and blood-to-plasma concentration ratio at equilibrium (32). Blood was divided into red blood cell and plasma compartments; tissues were divided into red blood cells residing in the tissue, an extracellular compartment (combined plasma and interstitial fluid) and the cellular tissue. Systemic metabolism was assumed to occur in the liver only. Renal or biliary excretion of unchanged CsA is negligible and was therefore not considered in the current model (33,34). Simulations in rat and human reported previously (19,20) were successfully reproduced to ensure that model implementation and scaling to human was performed adequately (data not shown). A stiff solver (ODE23s) was used to solve the set of ordinary differential equations applied in the current PBPK model to allow accurate numerical integration of rapidly and slowly changing rate equations.

$$V_{Li} \cdot Hct \cdot fvv_{Li} \cdot \frac{dC_{BC_{Li}}}{dt} = Q_{Li} \cdot Hct \cdot (C_{BC_{in}} - C_{BC\,Li}) \quad (2)$$

$$+ V_{Li} \cdot fvv_{Li} \cdot PS_{BC} \cdot \left(fu_p \cdot fcv_{Li} \cdot C_{E_{Li}} - Cu_{BC}\right)$$

$$Cu_{BC} = 0.5 \cdot \left[C_{BC} - K_{D,BC} - nP_T + \sqrt{\left(C_{BC} - K_{D,BC} - nP_T\right)^2 + 4 \cdot K_{D,BC} \cdot C_{BC}} \right] \quad (3)$$

$$V_{Li} \cdot [fvv_{Li} \cdot (1 - Hct) + fvic_{Li}] \cdot \frac{dC_{E_{Li}}}{dt} = Q_{Li} \cdot (1 - Hct) \cdot \left(C_{p_{in}} - C_{p_{Li}}\right) - V_{Li} \cdot fvv_{Li} \cdot PS_{BC} \cdot \left(fu_p \cdot fcv_{Li} \cdot C_{E_{Li}} - Cu_{BC}\right) - PS_{Li} \cdot \left(fu_{I_{Li}} \cdot fci_{Li} \cdot C_{E_{Li}} - fu_{T_{Li}} \cdot C_{NB_{Li}}\right) \quad (4)$$

$$\begin{aligned} &V_{Li} \cdot (1 - fvic_{Li}) \cdot \frac{dC_{NB\,Li}}{dt} = \\ &PS_{TC\,Li} \cdot \left(fu_{I_{Li}} \cdot fci_{Li} \cdot C_{E\,Li} - fu_{T\,Li} \cdot C_{NB_{Li}}\right) \\ &- k_{on\,Li} \cdot fu_{T\,Li} \cdot C_{NB_{Li}} \cdot (Bt_{Li} - C_{SB\,Li}) + k_{off\,Li} \cdot C_{SB\,Li} \\ &- CL_{int,H} \cdot fu_{T\,Li} \cdot C_{NB_{Li}} \end{aligned} \quad (5)$$

$$V_{Li} \cdot (1 - fvic_{Li}) \cdot \frac{dC_{SB\,Li}}{dt} = k_{on\,Li} \cdot fu_{T\,Li} \cdot C_{NB_{Li}} \cdot (Bt_{Li} - C_{SB\,Li}) - k_{off\,Li} \cdot C_{SB\,Li} \quad (6)$$

where V_{Li} and Q_{Li}, volume (L) and blood flow (L/h) of the liver tissue; C and Cu, total and unbound drug concentration in blood cells (BC), extracellular fluid (E), plasma (p) and hepatic inlet (in) (μg/L); NB, non-saturable binding sites; SB, saturable binding sites; Hct, hematocrit (0.45); fvv_{Li}, vascular fraction of the tissue (0.115); $fvic_{Li}$, interstitial fraction of the tissue (0.163); PS, permeability-surface area product in blood cells (BC) and tissue (T) (L/h); fu, fraction not bound to plasma (p), interstitial (I), liver tissue (Li) proteins (scalar); fcv_{Li}, coefficient to convert between extracellular and plasma concentration; fci_{Li}, coefficient to convert between extracellular and interstitial fluid concentration; k_{on} and k_{off}, on- and off-rates ($mL^2/(\mu g.h)$ and mL/h, respectively); Bt_T, total binding sites (μg-eq./mL); $CLint_H$ intrinsic hepatic clearance (L/h) , K_D (binding affinity constant)

Parameter estimation was performed using data from two healthy populations to obtain the hepatic intrinsic clearance ($CLint_H$) of CsA (11,35). Optimization of $CLint_H$ was performed using weighted nonlinear least-squared regression analysis (toolbox LSQ nonlin) in Matlab v. 7.12 by fitting the model to both sets of data (at doses of 1.5 and 2.5 mg/kg) simultaneously. To ensure that the optimization routine resulted in the global minimum, different initial estimates (above and below the anticipated posterior) were investigated to ensure all converged to the same final parameter estimate of $CLint_H$. Only positive solutions were allowed and no upper limit was imposed. The criterion for selecting clinical studies for validation of the model was that they reported administration of oral dosage forms (Sandimmune® and Neoral®) in addition to the intravenous dose in the same population, allowing a step-wise investigation of the PBPK model performance to predict first CsA i.v. and then oral concentration-time profiles. Model performance with optimized $CLint_H$ values was assessed against four independent studies reporting intravenous administration of CsA (36–39) by comparing the model predicted against observed CsA blood concentrations. Studies included in this assessment quantified CsA blood concentrations using assays with either absolute specificity for CsA (HPLC) or showed low cross-reactivity for CsA metabolites (EMIT and RIA) (40) and good correlation to HPLC methods. In total, 59 mean blood concentrations were included in this analysis; prediction success was assessed on the coefficient of determination, the slope of predicted *vs.* observed concentrations and the percentage of predictions within 2-fold of the observed value.

PBPK Modeling of CsA in Human After Oral Dose

The PBPK model defined above was extended to enable assessment of the concentration-time profiles after an oral dose. Kawai *et al.* (1998) used a first-order absorption model with a lag time to describe the oral concentration-time profiles of CsA with good accuracy (19). The absorption model applied in the current study was based on the compartmental absorption and transit model (23), to allow mechanistic description of the changes in local concentrations in the enterocytes and subsequent assessment of CsA interaction potential against intestinal CYP3A4, P-gp and BCRP (Eq. 10). The absorption model included a term of intestinal loss of CsA ($1\text{-}F_G$) and movement of drug from the enterocytes into the splanchnic blood supply was based on the Q_{Gut} model (41,42). Drug jejunal permeability reported previously in human (43) was used to calculate absorption rate constants in the different intestinal segments (Eq. 12); dissolution was taken into account (Eqs. 13 and 14)

$$\frac{dA_{St}}{dt} = -A_{St} \cdot Kt_{St} \quad (7)$$

$$\frac{dA_{G,1}}{dt} = +A_{St} \cdot Kt_{St} - A_{G,1} \cdot Kt_{G,1} - A_{G,1} \cdot ka_{G,1} \quad (8)$$

$$\frac{dA_{G,n}}{dt} = A_{G,n-1} \cdot Kt_{G,n-1} - A_{G,n} \cdot Kt_{G,n} - A_{G,n} \cdot ka_{G,n} \quad (9)$$

$(n=2\text{–}6)$

$$Vent_n \cdot \frac{dC_{ent,n}}{dt} = F_G \cdot \left(A_{G,n} \cdot ka_{G,n}\right) - C_{ent,n} \cdot Q_{Gut,n} \quad (10)$$

$$\frac{dA_{loss}}{dt} = (1 - F_G) \cdot \left(A_{G,n} \cdot ka_{G,n}\right) \quad (11)$$

$$ka = \frac{2 \cdot P_{eff}}{r_{SI}} \quad (12)$$

$$\frac{dA_{un,n}}{dt} = A_{un,\,n-1} \cdot Kt_{n-1} - A_{un,\,n} \cdot Kt_n - \frac{3D}{\rho \cdot r \cdot h} \cdot A_{un,n} \cdot \left(C_{S,n} - \frac{A_{dis,n}}{V_n}\right) \quad (13)$$

$$\frac{dA_{dis,n}}{dt} = A_{dis,\,n-1} \cdot Kt_{n-1} + \frac{3D}{\rho \cdot r \cdot h} \cdot A_{un,n} \cdot \left(C_{S,n} - \frac{A_{dis,n}}{V_n}\right) - A_{dis,\,n} \cdot Kt_n - A_{dis,\,n} \cdot k_{a,n} \quad (14[1])$$

The applied absorption model outlined in detail in our previous work (22) was applied here with minor alterations; in short, the small intestine was divided into 6 compartments (1 for duodenum, 2–3 for jejunum and 4–6 for ileum) for the intestinal lumen and enterocytes. A colonic compartment was also included and absorption was allowed to occur in the upper part of the colon. While clinical data indicate that the main absorption sites are the duodenum and jejunum, absorption from the colon was comparable to that of the ileum (44) and may therefore be of importance for CsA Sandimmune®. For this formulation the percentage of dose absorbed in the colon was approximately 4% while for CsA Neoral® absorption was nearly complete before intestinal contents reached the colon and colonic contribution to absorption was practically non-existent. Dissolved and undissolved drug in the lumen of the small intestine were modeled using previously defined rate equations (45). Additional parameters required for intestinal absorption relating to physiology were volumes of intestinal lumen and enterocytes as well as intestinal transit rate constants. Summary of CsA relevant parameters including solubility, particle radius, effective permeability and intestinal availability is provided in the Supplementary Material Table SV. The use of human intestinal fluid solubility under fasted conditions (46) considerably under-estimated the fraction of CsA Neoral® absorbed (23%) in our previous analysis (22). Keeping the intestinal solubility constant (16 mg/L) and optimizing P_{eff} was considered inappropriate, as an unrealistically high P_{eff} value was required to recover the oral concentration-time profiles; the value was in excess of 10 μm/s which has been reported for highly permeable drugs (47). Subsequently, optimization of solubility was performed by fitting the oral PBPK model to the oral blood concentration-time profiles reported for cyclosporine Sandimmune® (35) and Neoral® (11). Prediction success of the model with optimized solubility values was assessed for CsA Sandimmune® and Neoral® on four single dose studies each fulfilling the same selection criteria as for the i.v. data. In addition, simulations of steady-state profiles were performed using four and three studies following administration of Sandimmune® and Neoral®, respectively. Simulations were performed over a seven day dosing period to attain stead-state conditions following the dosing regimen specified in the clinical studies.

PBPK Model Sensitivity to Parameter Variability

A number of parameters may lead to changes in the CsA blood concentration-time profiles and some of which may also affect the unbound concentration and in turn the interaction potential of CsA against either transporters or metabolic enzymes. First and foremost, large discrepancy exists in the literature regarding the unbound fraction of CsA in human plasma (Supplementary Material). The most reliable methods to estimate CsA fu_p are equilibrium dialysis in stainless steel chambers (good recovery and reproducibility, most widely used) and ultracentrifugation. However, both methodologies resulted in different estimates of fu_p (1.5 or 6%, respectively). The reasons for these differences are unclear and consequently an intermediate value of 3% was used in the current assessment. An assessment of model sensitivity to parameter uncertainty was performed using the values of 1.5 and 6%. Additionally, the impact of variability in hematocrit, PS_{BC}, $CLint_H$ and F_G was investigated. The hematocrit has been shown to be reduced in transplant patients (14) and therefore simulations using values of 25 and 35% in addition to the simulations under normal conditions (45%) were explored. For hepatic intrinsic clearance and intestinal availability, variability

[1] C, A, K and ka, refer to concentrations, amounts, transit rate- and absorption rate constants in stomach (St), duodenum (G,1) and remaining intestinal segments n (G,n); V_{ent} and V, refer to the volumes of the enterocyte and intestinal lumen in compartment n; Q_{Gut}, refers to hybrid function of blood flow and drug permeability; dissolved (dis) and undissolved (un) drug in the intestinal lumen were modeled using diffusion constant (D), particle density and radius (ρ and r); effective diffusion layer thickness (h) and drug solubility (C_S). Modeling of intestinal metabolism based on *in vitro* clearance data failed and consequently intestinal metabolism was modeled semi-mechanistically by incorporating the term F_G (Eq. 10).

of +/− 30% and +/− 35%, respectively were assessed in addition to the mean values of 780 L/h (estimated in this study) and F_G=0.44 (22,48), respectively.

Simulation of the Time Course of CsA Interaction Potential Against Major Transporters/Metabolic Enzymes

PBPK model simulations of CsA interaction potential with respect to time against a number of uptake and efflux transporters were performed after a single oral doses of 380 mg Neoral® and 570 mg Sandimmune® administered to healthy volunteers (11,35). In addition, for CsA Neoral® the interaction potential at steady-state was assessed; in all cases CsA was assumed to be a competitive inhibitor (Eq. 15) of the transporters investigated and/or CYP3A4. This is a reasonable assumption for CYP3A4 where CsA has been reported to be a competitive inhibitor of a number of probe substrates (midazolam and fluticazone were exceptions as non-competitive inhibition was observed) (49). Assumption of either reversible inhibition mechanism results in the same theoretical interaction potential (Eq. 15); however, quantitative prediction of a specific DDI may be sensitive to the inhibition mechanism. The differences will be apparent for drugs with high unbound concentrations relative to their Km values for either transporter or metabolic enzyme. This is not the case for the specific example studied here (repaglinide), as uptake and metabolism occur under intrinsic conditions (i.e., Cu<< Km). The example of the rate equation implemented in the PBPK model for the assessment of CsA interaction potential is illustrated in Eq. 16, obtained by differentiation of Eq. 15 with respect to time. The equations highlight the importance of not only exposure and potency of the inhibitor for a specific process, but also the contribution of that process to the distribution of a victim drug into eliminating organ, as defined by the f_T parameter. Inhibitor mediated changes in drug distribution into non-eliminating organs would result in changes in V_{SS} and consequently the concentration-time profile, with no change in drug exposure (AUC).

$$\frac{1}{R} = \sum_{i}^{n} \frac{f_{T,i}}{1 + \sum_{j}^{m} \frac{[I]_{u,j}}{IC_{50,j,i}}} + 1 - \sum_{i}^{n} f_{T,i} \tag{15}$$

$$\frac{d\frac{1}{R}}{dt} = \sum_{i}^{n} \frac{-f_{T,i} \cdot \sum_{j}^{m} \frac{d[I]_{u,j}/dt}{IC_{50,j,i}}}{\left(1 + \sum_{j}^{m} \frac{[I]_{u}}{IC_{50,j,i}}\right)^{2}} \tag{16}$$

where 1/R describes the fraction of transporter or enzyme activity remaining in the presence of inhibitors j and transporters i; f_T, fraction of total hepatic uptake mediated by a transport protein i; $[I]_u$, inhibitor concentration-time profile at the relevant side of action; IC_{50}, inhibitor concentration which results in 50% reduction of the activity of transporter/enzyme *in vitro*.

Depending on the location of the processes involved, different input concentrations were used to study the theoretical interaction potential of CsA: the unbound hepatic inlet concentration (uptake transporters), liver intracellular concentration (efflux transporters and CYP3A4) and enterocytic concentration (efflux transporters and CYP3A4) along the small intestine. The IC_{50} values for the hepatic uptake transporters OATB1B1, OATP1B3 and OATP2B1 were obtained in the current study and were used in the PBPK analysis of the DDI potential. For NTCP, P-gp, BSEP, MRP2 and BCRP the IC_{50} values of 0.37, 1.66, 1.44, 3.45 and 3.36 μM, respectively were applied for the analysis; these estimates were based on literature collation provided in Supplementary Material Table SI. In the case of CYP3A, substrate-dependent IC_{50} values were reported (0.20 and 2.79 μM using repaglinide and midazolam as probes, respectively; both values were used in the analysis).

Incorporation of the Main CsA Metabolite, AM1 into the Prediction of DDI

Considering that AM1 blood concentrations can exceed those of CsA following single or multiple drug administration, this metabolite was of prime interest in the assessment of the overall interaction potential. The possible contribution of AM1 to the CsA DDI potential was assessed using reported blood concentration-time profiles of AM1 after a single and multiple oral doses of CsA (10,11). The contribution to the interaction potential was based on the unbound plasma concentration of AM1; the fu_p and B:P values for AM1 (0.034 and 3.0, respectively) were taken from the literature (14). In addition to AM1, other metabolites (AM9, AM1c and AM4N) exceed 25% of CsA AUC at steady state (10), as summarized in Table II. These metabolites of CsA were not commercially available at the time of the study and the *in vitro* inhibitory potency against uptake transporters could not be investigated. To assess the combined interaction potential of all CsA metabolites and considering their structural comparability we have assigned the same OATP IC_{50} values as obtained for AM1 to the remaining metabolites. These were used in conjunction with the corresponding reported metabolite blood concentrations following single CsA dose and at steady-state in order to investigate potential contribution of metabolites to CsA DDI potential. Unbound plasma concentrations were calculated using the tabulated blood to plasma concentration ratios (for the metabolites this ratio was assumed to be concentration independent, i.e. a constant value) and the fu_p (Table II).

Table II Percentage of AM9, AM4N, AM1c and AM19 Blood AUCs Relative to CsA and AM1 at Steady-State; Collation of Fraction Unbound in Plasma and Blood to Plasma Concentration Ratio

	% of AUC at steady-state[a]		fu_p (%)[b]	B:P[b]
	CsA	AM1		
CsA	100	27.9	3	non-linear
AM1	360[c]	100	3.4	3
AM9	112	31	3.1	3
AM4N	34.5	9.6	2.7	1.25
AM1c	41	11.4	n/a[d]	n/a[d]
AM19	23.5	6.6	n/a[e]	n/a[e]

[a] Bauer *et al*. (2003)

[b] Awni *et al*. (1989)

[c] single dose: the CsA to AM1 unbound $C_{max,plasma}$ ratio is 2.6-fold (or 3.0-fold when the CsA $C_{max,inlet}$ is used) and the unbound $AUCu_{0\text{-}24}$ of AM1 is 113% of that of CsA. At steady state, the CsA to AM1 unbound $C_{max,plasma}$ ratio is 1.3-fold (or 1.6-fold when the CsA $C_{max.inlet}$ is used) and the unbound $AUC_{0\text{-}tau}$ of AM1 is 206% of that of CsA

[d] Using the data of AM1

[e] Not considered as AUC <25% of CsA

Quantitative Prediction of Cyclosporine-Repaglinide DDI Using Dynamic PBPK Modeling

The current model for CsA was combined with a PBPK model of repaglinide described elsewhere (50). In short, repaglinide tissue distribution was predicted using mechanistic equations (51) for all tissues, with the exception of liver. For the liver, a two-compartment model was constructed separating the liver into extracellular space and liver tissue where exposure of liver tissue was determined by a passive diffusion clearance (P_{diff}), an active uptake clearance (V_{max}/K_m) and tissue binding (fu_{Li}) reported in the literature (24). An empirical scaling factor was applied to *in vitro* uptake V_{max} as specified elsewhere (50). Contribution of OATP1B1 to the overall uptake of repaglinide was estimated using the reported repaglinide concentration-time data in polymorphic individuals, analogous to the approach used previously for the estimation of fm_{CYP2D6} (52), as illustrated in Eq. 17.

$$f_{T,OATP1B1} = 1 - \frac{AUC_{TT}}{AUC_{CC}} \quad (17)$$

where AUC_{TT} and AUC_{CC} represent repaglinide AUC values reported in subjects with *SLCO1B1* 521TT and 521CC genotype, respectively.

Based on the polymorphic clinical data, contribution of OATP1B1 was estimated to be 49.6%; the value represents a weighted mean from 4 clinical studies, with the total number of 112 TT and 46 CC subjects (53–56). In the current analysis, the remaining 50% of repaglinide uptake were attributed to OATP1B3, based on in house kinetic data in HEK-OATP1B1 and HEK-OATP1B3 cells. The *in vitro* uptake parameters (P_{diff} and V_{max}) were scaled to *in vivo* using a hepatocellularity of 120×10^6 cells/g of liver. The intestinal absorption and metabolism was modeled using a compartmental absorption and transit model defined elsewhere (22). Metabolism of repaglinide was mediated by CYP3A4, CYP2C8 and UGTs in the liver (25) and by CYP3A in the small intestine (42). Scaling of the liver metabolism from *in vitro* data was performed using a hepatocellularity of 120×10^6 cells/g of liver and intestinal metabolism by regional CYP3A contents (9.7, 38.4 and 22.4 nmol for the duodenum, jejunum and ileum (57), respectively). The in silico interaction study between CsA and repaglinide was performed using the specifications of the clinical study; i.e., an oral dose of 100 mg CsA Neoral® administered 13 and 1 h before a 0.25 mg dose of repaglinide (58). In order to assess the impact of dose staggering on the DDI potential, simulations were performed using the following schedule: administration of repaglinide dose at −2, −1, −0.5, 0, +1, +2, +3 and +6 h relative to the second dose of 100 mg CsA. The impact of different timing of repaglinide dose on its AUC, C_{max} and F_G was investigated.

For the relevant processes (hepatic uptake and liver and intestinal metabolism), K_m values were modified by Eq. 16 to incorporate a dynamic change of repaglinide uptake and metabolic intrinsic clearances in response to changes in CsA concentrations over time. The IC_{50} values obtained against hepatic uptake transporters in the current study were used. For CYP3A4 metabolism, an IC_{50} value of 0.2 μM was used determined by the original investigators, as this assessment was based on the formation of M1 (CYP3A) from repaglinide, whereas the formation of M4 (CYP2C8) was not affected by CsA (58).

RESULTS

Assessment of CsA and AM1 IC_{50} Values *In Vitro*

IC_{50} data for CsA and AM1 were obtained in OATP1B1, OATP1B3 and OATP2B1 transfected HEK cells before and after a preincubation of 30–45 min. Representative IC_{50} plots are shown in Fig. 1 and the individual IC_{50} plots and values can be found in the Supplementary Material Figure SI and Tables SVII and SVIII. Without pre-incubation, CsA exhibited comparable potencies against OATP1B1 and OATP1B3 (0.20 and 0.16 μM, respectively), whereas AM1 was a more potent inhibitor of OATP1B3 than -1B1 (0.19 *vs.* 0.4 μM) (Table III). Following pre-incubation, a significant left shift in the IC_{50} plots was observed for both CsA and AM1 against OATP1B1 and OATP1B3 (Fig. 1). After pre-incubation, CsA IC_{50} values decreased to 0.019 and

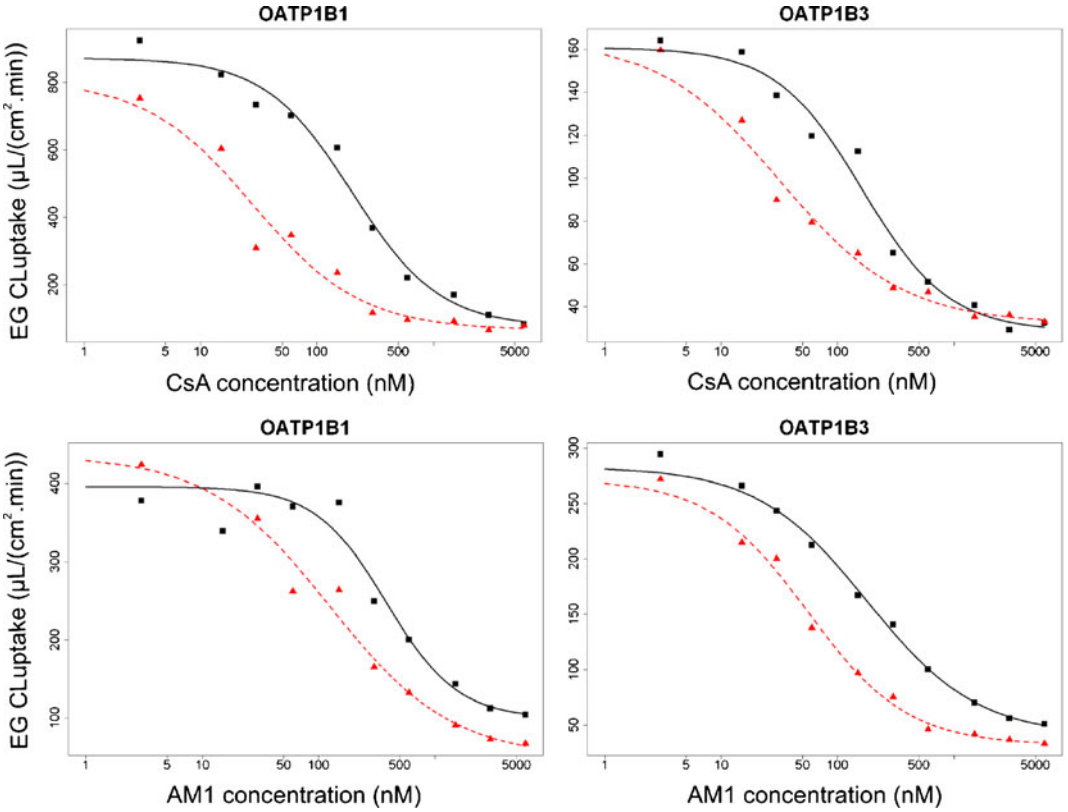

Fig. 1 Representative IC_{50} plots of CsA and AM1 against OATP1B1 and OATP1B3 in transiently transfected HEK-293 cells; data before (■) and after (▲) pre-incubation are the mean of duplicates and the lines represent the fits of Eq. 1 to the data; solid and dashed lines for data before and after pre-incubation.

0.032 µM for OATP1B1 and OATP1B3, respectively. AM1 IC_{50} estimates displayed similar trends regarding the pre-incubation step and were reduced to 0.093 and 0.060 µM, respectively. No IC_{50} values could be determined against OATP2B1; at the highest CsA concentration investigated (6 µM), OATP2B1 activity was reduced to approximately 50% of control, while no effect was observed for AM1.

Table III Mean IC_{50} Data (±SD, n=3–4) for CsA and Its Primary Metabolite AM1 with and without 30 Minute Pre-incubation in Transiently Transfected HEK293 Cells

Transporter	IC_{50} (without pre-incubation)	IC_{50} (with pre-incubation)
	µM	
CsA		
OATP1B1	0.198 ± 0.069	0.019 ± 0.007
OATP1B3	0.162 ± 0.056	0.032 ± 0.003
OATP2B1	~50% activity at 6 µM	~50% activity at 6 µM
AM1		
OATP1B1	0.411 ± 0.161	0.093 ± 0.023
OATP1B3	0.191 ± 0.062	0.059 ± 0.015
OATP2B1	–	–

–no inhibition observed at the highest AM1 concentration (6 µmol/L)

No apparent differences were observed in the uptake clearance of [^{3}H]-estradiol 17β-D-glucuronide before and after pre-incubation (fits for both conditions converge to the same uninhibited uptake clearance). The same applies for the passive diffusion clearance as baseline $CLint_{uptake}$ values in the presence of high inhibitor concentrations were comparable in both conditions, as was the CsA recovery.

Simulation of CsA Blood Concentration-Time Profiles After Intravenous Drug Administration

Mean CsA concentration-time profiles previously reported in healthy volunteers administered 1.5 and 2.5 mg/kg as an i.v. infusion over 3 h were successfully simulated from the tissue distribution data in rat with the relevant physiological information for human using a $CLint_H$ value of 780 L/h. The simulated blood and plasma concentration-time profiles are shown in Fig. 2a. Correlation between observed and predicted data was high for the two datasets used after optimization of $CLint_H$ (R^2=0.956). The PBPK model was further validated using a set of four independent studies across different populations (healthy volunteers and transplant patients) with CsA doses ranging from 62.3 to 256 mg administered over an infusion period of two to three hours (Table IV). The diagnostic goodness of the fit plot is shown in Fig. 2b. A high degree of

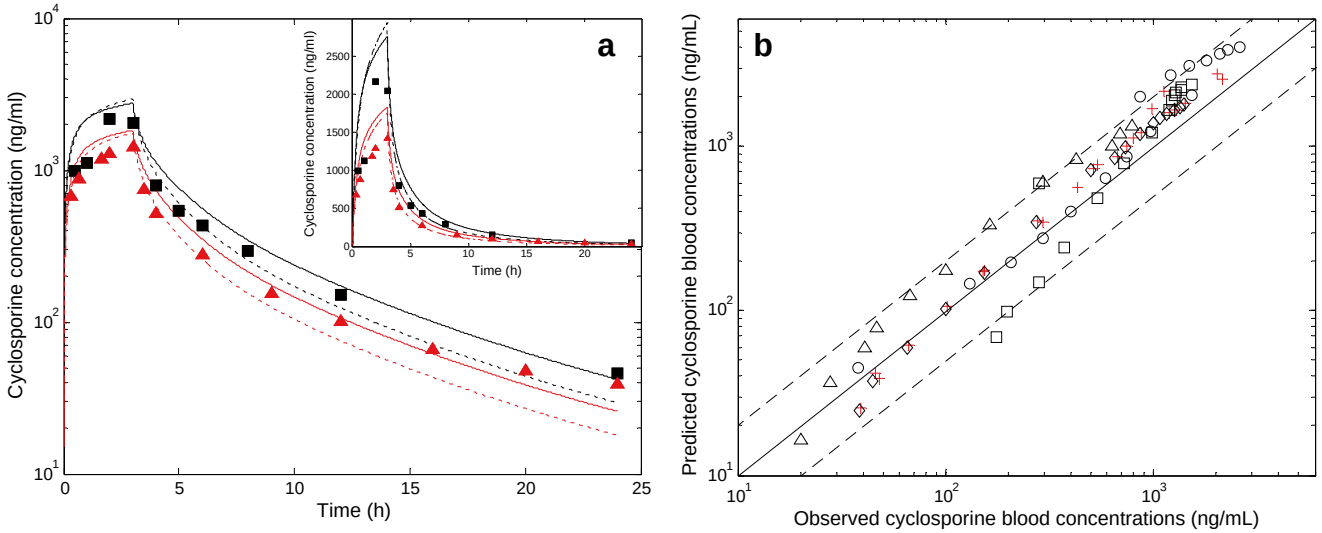

Fig. 2 (**a**) predicted (solid lines) and observed (symbols) mean blood concentration-time profiles of CsA following parameter optimization of $CLint_H$; (■) Ducharme *et al*. (1995) 2.5 mg/kg and (▲) Ku *et al*. (1998) 1.5 mg/kg; dashed lines represent the simulated plasma concentration-time profiles; (**b**) log-log plot of predicted *vs*. observed mean CsA concentrations after i.v. dose from 4 independent studies (in black) and the two studies used for optimization of $CLint_H$ (+); solid line represents line of unity and dashed lines indicated deviation by 2-fold from the line of unity; ○, □, ◊ and Δ represent data from separate clinical studies as specified in the Supplementary Material Table SIX.

correlation was observed for this dataset (R^2=0.943, n=59) with 88% of the concentrations predicted within 2-fold of the line of unity; the PBPK model showed a minor but consistent trend to over-predict CsA blood concentrations (36%). Details of the clinical studies used for the PBPK model validation are outlined in the Supplementary Material Table SIX.

Simulation of CsA Blood Concentration-Time Profiles After Oral Drug Administration

Prediction of CsA Sandimmune® and Neoral® concentration-time profiles was performed for two studies which reported i.v. and oral data in the same individuals (11,35). Use of CsA solubility determined in fasted human intestinal fluids underestimated the CsA concentration-time profiles and the fraction absorbed considerably (22). Consequently, optimization of solubility was performed within the PBPK model implemented here. The solubility required to recover the observed oral blood concentration-time profiles of CsA following Sandimmune® and Neoral® formulations were 32 and 140 mg/L, respectively; these being within the range of reported solubility in human intestinal fluids after fasted and fed conditions (16–248 mg/L) reported elsewhere (46). Simulations of the oral concentration-time profiles of CsA with the optimized solubility are shown in Fig. 3a for Sandimmune® and in Fig. 4a for Neoral®. For both formulations the PBPK model performance was assessed against data from four independent studies (Table IV). For Sandimmune® single dose, a bias towards over-predictions was observed, particularly at low concentrations (absorption phase rather than terminal phase). The coefficient of determination was reduced in comparison to the i.v. data (R^2=0.733) and 77% of predicted values were within 2-fold of unity (Fig. 3b). For Neoral® single dose, no prediction bias was observed and the degree of correlation was high (R^2=0.909) with 89% of the predicted values within 2-fold of unity. Less clinical data were available at steady state for both Sandimmune® and Neoral® in comparison to single dose. A comparable prediction success was observed for CsA at steady-state, as illustrated in Table IV and Figs. 3c and 4c for Sandimmune® and Neoral®, respectively. Individual analyses and additional information of the clinical studies can be found in the Supplementary Material Table SX and SXI.

Table IV Summary of PBPK Model Performance After Intravenous and Oral Doses of CsA to Human[a]

	i.v.	oral			
		Sandimmune®		Neoral®	
		Single	Steady-state	Single	Steady-state
n (studies)	4	4	4	4	2
n (individuals)	36	65	45	80	39
n (mean blood concentrations)	59	64	43	56	26
R^2	0.943	0.736	0.894	0.909	0.921
Predictions inside 2-fold (%)	88	77	98	89	81

[a] A summary of studies utilized in this assessment can be found in the Supplementary Material Tables SIX–XI

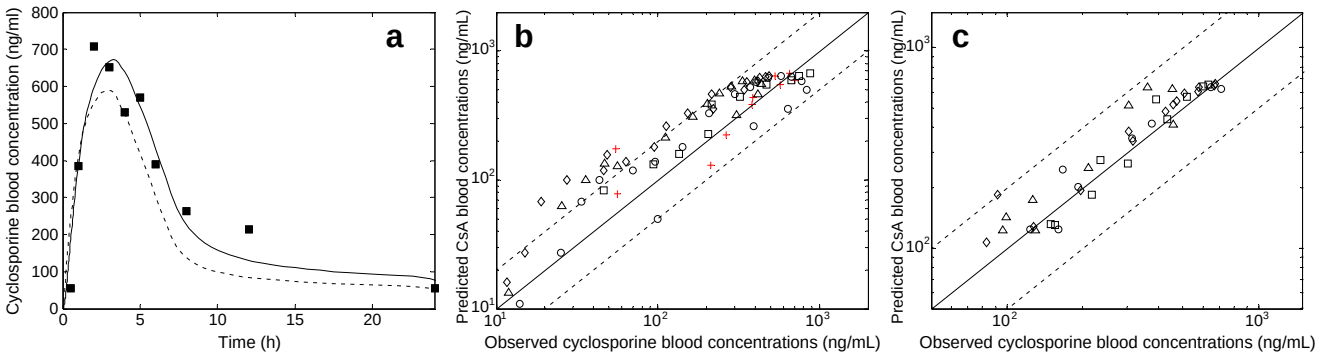

Fig. 3 Sandimmune®: (**a**) predicted (solid line) and observed (■) blood concentration-time profiles of CsA after a single oral dose (570 mg) following parameter optimization of drug solubility; dashed lines indicate the simulated hepatic plasma inlet concentration-time profile; (**b**), log-log plot of predicted *vs.* observed mean CsA concentrations after single oral doses reported in 4 independent studies (in black) and one study used for optimization of solubility (+); ○, □, ◊ and Δ represent data from separate clinical studies specified in the Supplementary Material Table SX; (**c**), log-log plot of predicted *vs.* observed mean CsA concentrations at steady state reported in 4 independent studies (in black); ○, □, ◊ and Δ represent data from separate clinical studies specified in the Supplementary Material (Table SX); solid line represents line of unity and dashed lines indicated deviation by 2-fold from the line of unity.

PBPK Model Sensitivity to Parameter Variability

An assessment of the model sensitivity to parameter variability identified minor differences in the predicted interaction potential due to changes in fu_p, hematocrit, PS_{BC}, cardiac output and body weight. This can be rationalized by the fact that the unbound concentration of CsA does not change in response to changes of any of the above parameters in isolation. However, total blood and plasma concentration-time profiles of CsA showed differential sensitivities to these changes (Supplementary Material Figure SII). In contrast, variability in hepatic intrinsic clearance and F_G had more pronounced effects on CsA unbound plasma or liver concentration and subsequently variations in these parameters are likely to affect magnitude of DDI of a victim drug with CsA. It is noteworthy that, while changes in fu_p did not result in a change in unbound plasma concentration-time profiles when $CLint_H$ was kept constant, the use of different fu_p values did result in variable parameter estimates of $CLint_H$ during optimization. Therefore, the overall uncertainty of fu_p in the literature reduces confidence in the true unbound concentration-time profile and consequently the magnitude of CsA interaction potential.

Interaction Potential of CsA and AM1 Against Hepatic Uptake Transporters

The PBPK model predicted blood concentration-time profiles of CsA Neoral® following a single (380 mg) and multiple CsA doses (110 mg every 12 h) are illustrated in Fig. 5. In addition,

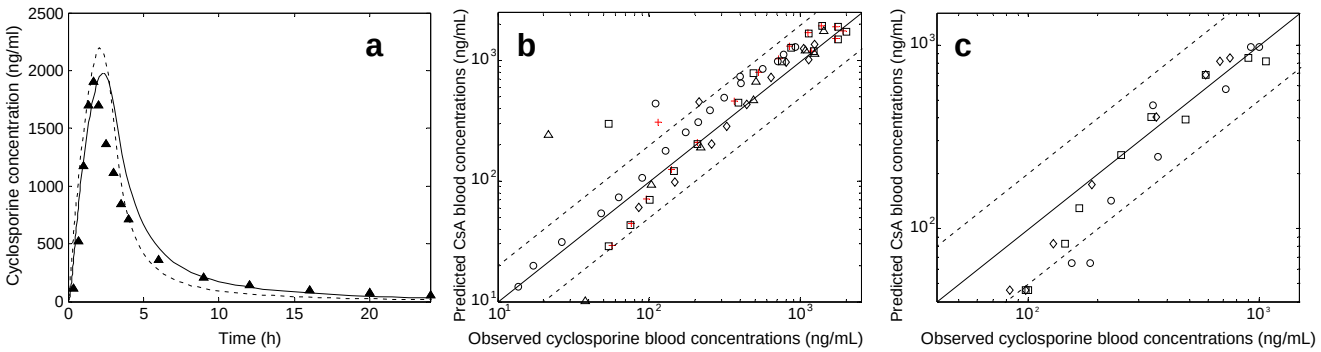

Fig. 4 Neoral®: (**a**), predicted (solid line) and observed blood concentration (▲) of CsA after a single oral dose (380 mg) following parameter optimization of drug solubility; dashed lines indicate the simulated hepatic plasma inlet concentration-time profile; (**b**), log-log plot of predicted *vs.* observed mean CsA concentration after single oral doses reported in 4 independent studies (in black) and one study used for optimization of solubility (+); ○, □, ◊ and Δ represent data from separate clinical studies specified in the Supplementary Material Table SXI; (**c**), log-log plot of predicted *vs.* observed mean CsA concentration at steady-state reported in 3 independent studies (in black) and one study used for optimization of solubility (red crosses); ○, □ and ◊ represent data from separate clinical studies specified in the Supplementary Material Table SXI; solid line represents line of unity and dashed lines indicated deviation by 2-fold from the line of unity.

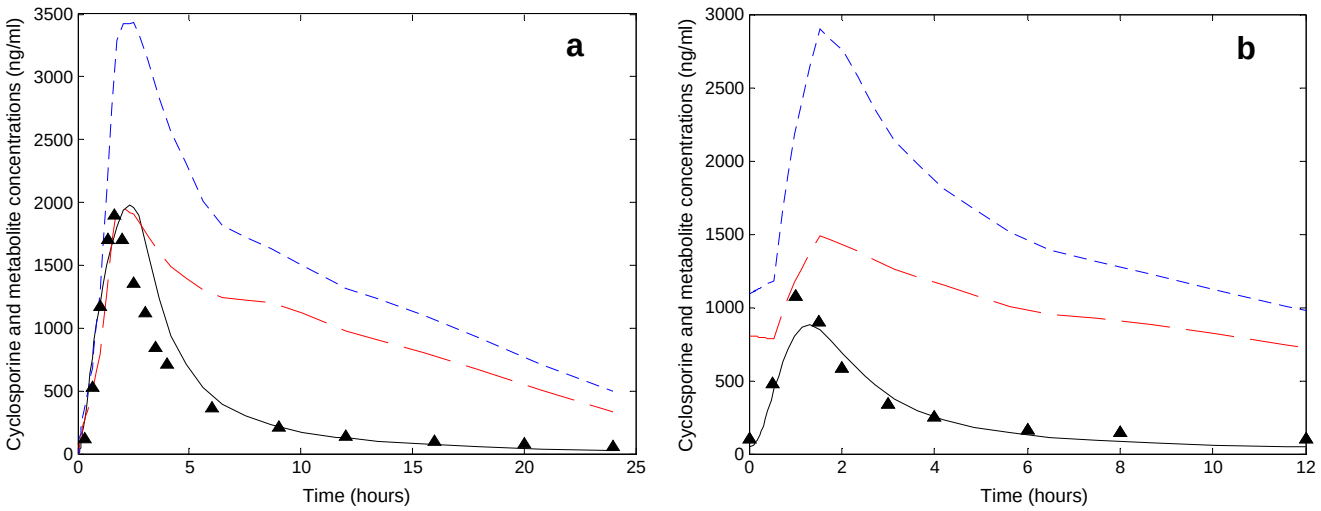

Fig. 5 (**a**) Observed and predicted CsA (▲ and solid line), observed AM1 (dashed red line) and total CsA metabolites (AM1 + AM9; dotted blue line) blood concentration-time profiles after a single oral dose (380 mg Neoral®, (11)); (**b**) Observed and predicted CsA (▲ and solid line), observed AM1 (dashed red line) and total CsA metabolites (AM1 + AM9 + AM4N + AM1c; dotted blue line) blood concentration-time profiles after multiple oral doses (110 mg Neoral® twice daily (10)).

Fig. 5 illustrates the reported total blood concentrations of AM1 and combined metabolite concentration after a single dose of CsA (AM1 and AM9) and at steady-state (AM1, AM9, AM4N and AM1c). The time course of the reduction in hepatic uptake transporter activity in the presence of CsA was investigated for these dosage regimens due to availability of both CsA and metabolite concentration-time data in the selected clinical studies (10,11). Simulations of the CsA and combined CsA and AM1 interaction potential following a single oral dose of 380 mg Neoral® are illustrated in Fig. 6a (OATP1B1) and B (OATP1B3) using the IC_{50} data obtained before and after pre-incubation. For a high, single oral dose of 380 mg Neoral®, the predicted maximal hepatic inlet concentrations of CsA was 2187 ng/mL (corresponds to Cu_{inlet} of 55 nM). Differences in the hepatic inlet and outlet concentrations were small due to the low hepatic extraction of CsA (approximately 20%). The maximal total plasma concentration in the hepatic inlet exceeded the systemic concentration by less than 20%. The OATP1B1 transporter activity is reduced to 26% of its basal activity; however, the duration of the maximal inhibitory effect is relatively short given the extensive distribution and elimination of CsA (Fig. 6a). A similar extent of interaction is apparent for OATP1B3; reduced activity of this transporter over time by CsA is shown in Fig. 6b. Use of the IC_{50} data following pre-incubation had a pronounced effect on the increase in the inhibition interaction potential for both transporters. Inclusion of the interaction potential of AM1 had a relatively minor impact on the overall DDI potential following single dose of CsA. Although total blood concentrations of AM1 are high, this metabolite is extensively distributed into red blood cells, resulting in an approximately 3-fold lower fu_b value in comparison to CsA. The lower maximal unbound concentrations and differences in potencies against OATP1B1 (0.093 *vs.* 0.019 μM for CsA) explain the minor contribution of AM1 to the maximal inhibition effect.

In contrast to the single dose study, the CsA dose for the steady-state data was considerably lower (110 mg every 12 h) and similar to typical maintenance conditions (100–200 mg). Based on this dose, the PBPK model predicted a reduction in OATP1B1 and OATP1B3 activities to 47 and 59% of control, respectively (Fig. 6c, d). Similarly, and despite the considerable accumulation of AM1 after multiple dosing (Fig. 5), the maximal interaction potential of CsA at steady state increased by a relatively small extent (<5%) when AM1 is taken into account (Fig. 6c, d); in this instance only the IC_{50} data following pre-incubation were considered in the analysis. Inclusion of the other metabolites (assuming the same potency as AM1) had a more pronounced effect on OATP1B3 in agreement with the *in vitro* potency data; the effect was more apparent during the terminal phase (Fig. 6d). Considering CsA alone and assuming reversible inhibition, the recovery of the uptake transporter was fast. Simulated reduction of transporter activity to <50% of the initial value for OATP1B1 and OATP1B3 was short (approximately 4 h), even when AM1 was included. In the case of Sandimmune®, the predicted magnitude of the inhibition was lower in comparison to Neoral® (Table V); however, because of the slower absorption of CsA from this formulation the duration of the inhibitory effect was more protracted (data not shown).

Interaction Potential of CsA Against Other Hepatic Processes

A summary of CsA interaction potential against a range of uptake and efflux transporters is provided in Table V. Even at the highest unbound liver tissue concentration, the reduction of individual efflux transporter activity (either P-gp, BSEP,

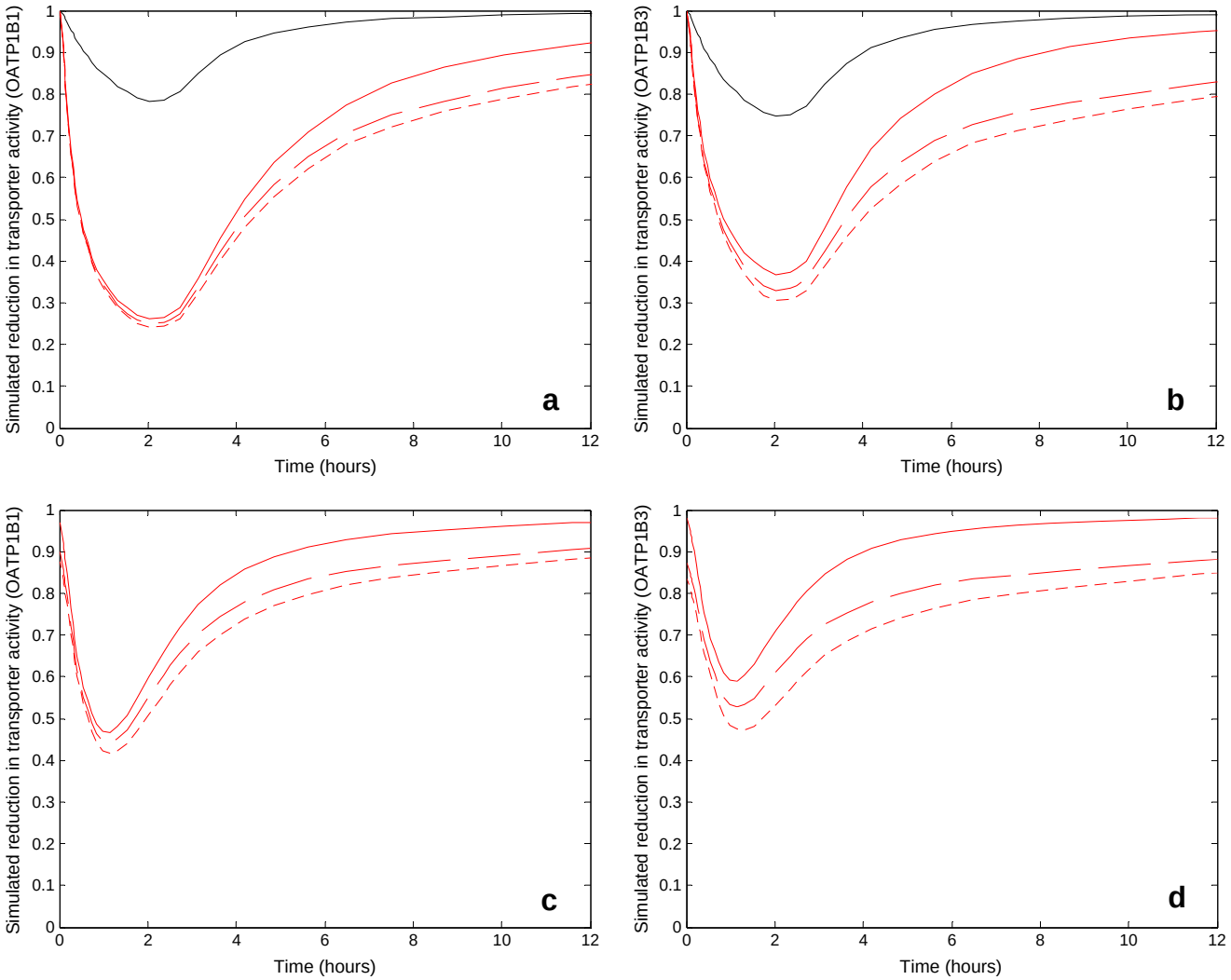

Fig. 6 Simulated interaction potential of CsA after single dose of 380 mg Neoral® (**a**, **b**), and after multiple oral doses of 110 mg twice daily Neoral® (**c**, **d**). (**a**, **c**) Interaction potential against OATP1B1 and B and D the interaction potential against OATP1B3. Simulations were performed using the IC_{50} values obtained before and after pre-incubation (black and red lines, respectively) and excluding (solid lines) or including AM1 (dashed lines) or total metabolite concentrations (dotted lines) in the assessment of interaction potential.

MRP2 or BCRP) by CsA is minor using available literature IC_{50} data (less than 5%, regardless of formulation) and seems unlikely to contribute to clinical DDIs. The predicted extent of CYP3A4 inhibition by CsA was dependent on the probe substrate used *in vitro* to assess CsA inhibitory potency. Use of midazolam inhibition data, predicted no more than 3% reduction in CYP3A4 activity, whereas the use of repaglinide estimates (based on formation of M1 metabolite as a CYP3A4 probe) resulted in a reduction of up to 26% of hepatic CYP3A4 in the presence of CsA.

Interaction Potential of CsA Against Intestinal Efflux and CYP3A4

The inhibition potential of CsA was also investigated at the level of the small intestine for a single dose of Sandimmune® (570 mg) and Neoral® (380 mg), as illustrated in Fig. 7a, b, respectively. Under the assumption that all CsA in the enterocytes is unbound, enterocytic CsA concentrations (3.6–6.7 μmol/L) exceeded unbound hepatic inlet concentrations by a considerable margin (60 to 120-fold). Consequently, the CsA interaction potential was high against all efflux transporters and CYP3A4 in comparison to the liver. For example, predicted P-gp activity was reduced by 48 and 80% for Sandimmune® and Neoral®, respectively, whereas up to 97% of CYP3A4 activity was inhibited (Table V). Analogous to liver, duration of the interaction effect was prolonged for Sandimmune® (Fig. 7); the magnitude of the reduction in transporter activity was dependent on the intestinal segment due to regional differences in blood supply and surface area available for absorption.

Table V Predicted Maximal Reduction in Transporter/Enzyme Activity in the Presence of CsA; Values in Parentheses Represent the Combined Contribution of CsA and AM1[a]

	Maximal reduction in transporter/ enzyme activity (%)			
	Liver		Intestine[b]	
	Sandimmune®	Neoral®	Sandimmune®	Neoral®
OATP1B1	43.1	73.9 (75.1)	n/a	n/a
OATP1B3	31.5	63.2 (67.0)	n/a	n/a
OATP2B1	0[c]	0[c]	n/a	n/a
NTCP	3.8	12.9 (16.5)	n/a	n/a
P-gp	< 1	3.0 (4.1)	33.1–48.1	68.2–80.3
BCRP	< 1	1.5 (2.1)	19.6–31.4	51.4–66.8
MRP2	< 1	1.5 (2.0)	19.2–30.9	50.8–66.2
BSEP	< 1	3.4 (4.7)	n/a	n/a
CYP3A4	6.4[d]	20.2 (26.4)[d]	80.4–88.5[e]	94.7–97.1[e]

[a] For processes where the IC_{50} of AM1 is unknown, the IC_{50} values for the metabolite and CsA were considered to be the same (only considered for Neoral® as AM1 concentration-time profiles were reported in the clinical study)

[b] At the level of the intestine only CsA is considered; interactions differ in different segment of the small intestine (range indicated)

[c] Could not be determined in the current study

[d] use of IC_{50} data obtained with repaglinide as probe substrate (worst case scenario; use of IC_{50} data obtained using midazolam as probe substrate resulted in <1% and 3% reduction in CYP3A4 activity for Sandimmune® and Neoral®, respectively)

[e] If IC_{50} data were based on midazolam as probe substrate a 22.7–35.6% and 56.0–70.8% reduction in CYP3A4 activity was predicted for Sandimmune® and Neoral®, respectively

Prediction of Clinical Interaction of Repaglinide

Finally, quantitative prediction of the reported DDI between CsA and repaglinide was performed by combining the respective PBPK models of the inhibitor and the victim drug. This prediction was performed utilizing only CsA considering the minor contribution predicted for AM1. The clinical interaction study was performed using an oral dose of 100 mg CsA Neoral® administered 13 and 1 h before a 0.25 mg dose of repaglinide (58). CsA concentration-time profile reported in the study was accurately reproduced by the current PBPK model (data not shown). The reported study design was applied for the simulations together with alternative dosing regimens to indicate conditions when maximum DDI would be predicted and when the DDI may be avoided. Following the dosage regimen reported in the clinical study, the PBPK modeling approach predicted a 1.9- and 1.8-fold fold-change in repaglinide AUC and C_{max}, respectively. Predictions were based on the assumption that repaglinide hepatic uptake is completely mediated via OATP1B1 and are in agreement with the reported changes in these parameters (Table I). Assuming an equal contribution (50%) of OATP1B1 and OATP1B3 to repaglinide active uptake, a comparable magnitude of DDI (1.75 and 1.7-fold change in AUC and C_{max} respectively) was predicted, given the similar potencies of CsA against OATP1B1 and OATP1B3. Figure 8a shows a comparison of the predicted and reported concentration-time profiles of repaglinide (control and CsA phase). The impact of dose staggering on the magnitude of CsA-repaglinide DDI is illustrated in Fig. 8b, where repaglinide dose is administered from −2 to +6 h relative to the

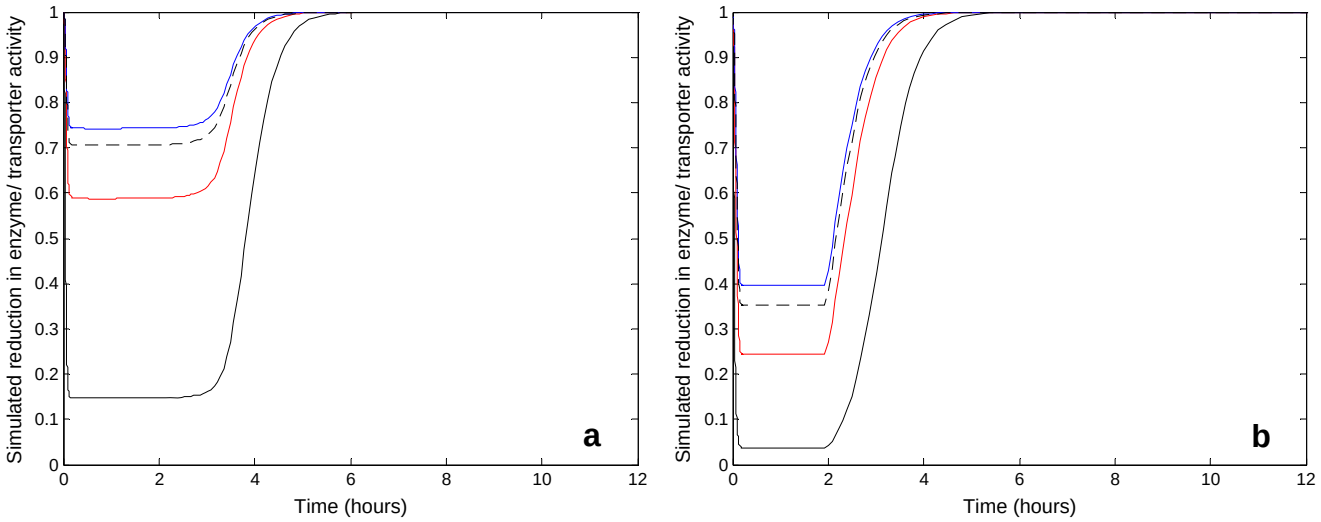

Fig. 7 Simulated interaction potential of CsA against intestinal efflux transporters, P-gp (red) and BCRP (blue), and CYP3A4 (black; solid line: repaglinide IC_{50}; dotted line: midazolam IC_{50}) in the proximal part of the small intestine; (**a**) interaction potential after a single dose of CsA Sandimmune® (570 mg) and (**b**) interaction potential after a single dose of CsA Neoral® (380 mg).

CsA dose; all the simulations are based on the 100 mg CsA dose, as reported in the clinical study. Maximal magnitude of DDI is predicted at +30 min. From the simulations it is apparent that a clinically relevant pharmacokinetic DDI (fold change in repaglinide AUC >1.25) may be avoided if repaglinide is either given 1 h before or 3 h after CsA (Fig. 8b). Despite complete inhibition of intestinal CYP3A4, its contribution to the magnitude of repaglinide DDI is expected to be minor (fold change in $F_G < 1.2$), considering the high intestinal availability of repaglinide under control condition ($F_G > 0.8$). Use of much higher CsA dose in the PBPK model (380 mg) under the same dosing regimen as in the clinical study (t=+1 h) predicted an increase in repaglinide AUC by 3.2-fold and in C_{max} by 2.3-fold.

DISCUSSION

Ability to assess and predict CsA transporter and metabolism interaction potential is of considerable importance given the large number of CsA mediated DDIs reported (Table I) and potential contribution of multiple interaction mechanisms. In the current study, the *in vitro* potency for CsA and its main metabolite AM1 were determined against the hepatic uptake transporters OATP1B1, OATP1B3 and OATP2B1 and CsA concentration-time profiles at the relevant sites of interest were generated using a validated PBPK model. Furthermore, availability of clinical data for AM1 and other metabolites allowed the assessment of their contributing role to the interaction potential after oral doses of CsA (single dose and steady state).

Assessment of IC_{50} Values of CsA

Previously, more than a 20-fold increase in CsA inhibitory potency against OATP1B1 was reported following a pre-incubation step (17). The effect of pre-incubation was confirmed in the current study using [^{3}H]-estradiol glucuronide as a probe substrate, although the observed shift in IC_{50} values was less pronounced (on average 12-fold for OATP1B1 and 5.2-fold for OATP1B3). The fold increase in CsA potency was highly variable between experiments and ranged from 5 to 21 in four paired OATP1B1 IC_{50} experiments (+/− pre-incubation); this behavior was not exclusive to OATP1B1 but was also evident for OATP1B3 and for CsA metabolite AM1 (average fold change in IC_{50} of AM1 after pre-incubation 3.3 and 4.8 for OATP1B3 and OATP1B1, respectively). The reasons for the IC_{50} shifts are currently unknown; whether this phenomenon is associated with a time-dependent inhibition mechanism requires further evaluation. Alternatively, possibility of inhibition at multiple binding sites of OATP1B1 cannot be ignored, considering reports of substrate-dependent inhibition of this transporter (59). In order to avoid bias due to substrate-dependent inhibition, vitro inhibition data should be obtained for the clinically relevant inhibitor-substrate pair whenever possible. It is unknown whether CsA exhibits similar effect on other transporters e.g., P-gp or BCRP. To our knowledge, no additional inhibition data for CsA metabolites against either uptake/efflux transporters or drug metabolizing enzymes have been reported in the literature. The current study did not observe more than 50% inhibition of OATP2B1 at the highest CsA/AM1 concentration investigated; this is in agreement with

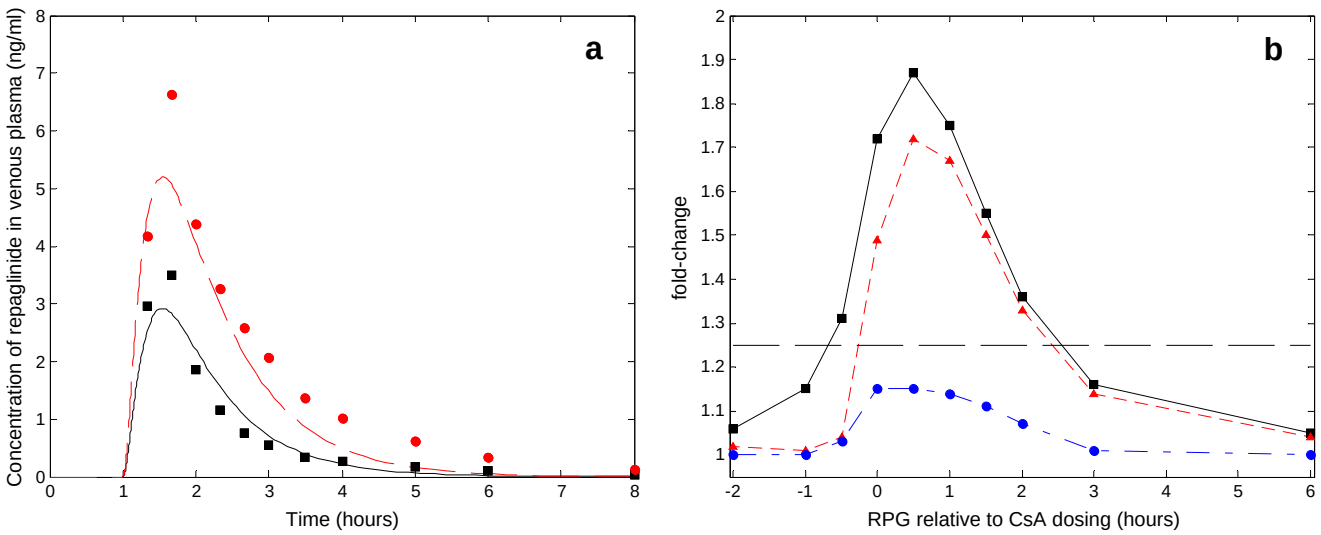

Fig. 8 (**a**) Observed (symbols) and predicted (lines) repaglinide plasma concentration-time profiles for control (black) and inhibitor phase (red) following CsA Neoral® dose of 100 mg 13 h and 1 h prior to a 0.25 mg dose of repaglinide; (**b**) fold-change in repaglinide AUC (black), C_{max} (red) and F_G (blue) in the presence of CsA when repaglinide is administered at −2 to +6 h relative to CsA.

another recent study (60), but contrary to an earlier report of high CsA potency (IC_{50} <0.1 μM) against this transporter (5).

CsA PBPK Model and Model Parameters

The distribution of CsA into rat tissue and blood has been extensively studied (19,21,61). The current analysis is based on the Tanaka model (20) which has not previously been used to predict CsA concentration-time profiles in humans. In preliminary work, reproduction of the scaling procedure suggested previously (19) was successful (data not shown) and was therefore implemented into the current assessment. The inclusion of complex tissue models in the PBPK modeling of CsA represents clear improvement to an earlier PBPK model for CsA which did not account for nonlinear blood and tissue distribution characteristics (21), illustrating that for this drug more extensive blood and tissue distribution data are required than simple tissue-to-blood and blood-to-plasma partitioning coefficients.

Prediction of CsA Concentration-Time Profiles

In the current analysis, hepatic intrinsic clearance ($CLint_H$) of CsA was estimated by fitting the PBPK model to the concentration-time profiles obtained after infusion of two different dose levels to healthy populations (11,35). In spite of the complexity of the model, optimization for a single parameter lead to a fairly good fit of the i.v. blood concentration-time profiles (Fig. 2). This indicates that the underlying tissue distribution characteristics obtained in rat and the subsequent scaling technique represent a valid approach to assess the overall distribution kinetics of CsA in humans. Evaluating the model against a number of i.v. studies was successful (Table IV). The i.v. PBPK model of CsA was subsequently extended to allow predictions of oral blood concentration-time profiles and mechanistic description of changes in CsA enterocytic concentrations along the length of small intestine. The performance of the oral PBPK model was better for CsA Neoral® than for the Sandimmune® formulation, which can be rationalized with the less variable data reported for the Neoral® formulation (62).

Assessment of CsA Interaction Potential with Respect to Time

Currently, predictions of transporter-mediated DDIs are based on the maximal unbound concentration entering the liver (3,4). These static models generally estimate hepatic inlet concentration based on observed C_{max} in conjunction with input from drug absorption parameters (defined by the k_a, F_a, dose of the inhibitor and the hepatic blood flow). If inhibitors show appreciable intestinal first-pass metabolism (as in the case of CsA), the inclusion of the parameter F_G is required as otherwise unrealistically high hepatic inlet concentrations are estimated. Shortcomings of this approach, such as the uncertainty of recommended values for k_a, F_a, Q_H, have previously been highlighted using the example of CsA (2). A recent study has extended the static liver model to accommodate multiple sites of interaction, assuming complete inhibition of either intestinal enzymes or transporters (resulting in inhibited F_aF_G=1), or by accounting for inhibition of both uptake and efflux in the liver (4). However, in all these approaches the static models are associated with a large number of assumptions and do not consider the concentration-time profile of the inhibitor. And although they may reduce the number of false negative predictions, these approaches should be considered only as a categorical tool, as they are inadequate for quantitative prediction of transporter DDIs.

For a drug like CsA, which has a large number of clinical DDIs with victim drugs associated with diverse ADME mechanisms (Table I), a mechanistic approach is needed to rationalize and predict these complex DDIs. Consideration of the time course of the inhibitor at the relevant sites of interaction (enterocytes, hepatic inlet and liver tissue) has been defined within the mechanistic framework of the current PBPK model. Evaluation against a number of clinical studies for both i.v. and oral drug administration provides confidence in the current model and its extrapolation to different doses and formulations (Supplementary Material Tables SX and SXI). In addition, the impact of AM1, the main CsA metabolite, was included into the current assessment of the interaction potential and prediction of DDIs. The assessment was important considering that a number of clinical studies report comparable or higher AM1 than CsA concentrations at steady state (10,12,15). This consideration was in line with the FDA recommendation to assess metabolites when the exposure exceeds 25% of the parent and was of relevance considering considerable potency of AM1 against OATP1B1/1B3. Assuming reversible inhibition mechanisms, simulations of the interaction potential suggest a relatively minor contribution of AM1 to the overall interaction potential of CsA (Fig. 6). This is not surprising considering the substantial distribution of AM1 into red blood cells and lower potency against OATP1B1/1B3 (Table II and III). It is noteworthy that the current blood to plasma concentration ratio and fu_p values of the metabolites are based on model fitting rather than experimental determination (14). Whether AM1 shows nonlinear blood distribution analogous to CsA is currently unknown. Unless other metabolites (e.g., AM9, AM4N or AM1c) show considerably higher potency than CsA it seems reasonable to assume that their contribution is negligible given that they attain lower blood concentrations than AM1 while displaying similar red

blood cells distribution and plasma binding (10,14). As no standards of these metabolites are commercially available at this time, their contribution to the observed clinical DDIs, however, cannot be ruled out. The current analysis highlights the need for careful interpretation of the role of metabolites in the DDI assessment. Proposed >25% of the parent exposure cut-off can in some cases be very misleading, as the overall reduction in transporter/enzyme activity will depend on the inhibition mechanism, relative potency and unbound concentration of each of the inhibitors at different sites of interaction, as illustrated here in the case of AM1. However, availability of either exposure or potency data for metabolite(s) during the early stages of drug development represents an issue.

The current data predicted negligible effects of CsA on hepatic metabolism via CYP3A4 or biliary excretion (Table V). There is minimal clinical evidence to support this prediction for the efflux transporters P-gp, BCRP and MRP2; however, data following i.v. administration of midazolam (marker of CYP3A4 activity) in the presence of CsA have been reported (63,64). The magnitude of DDI varies from no interaction to 1.3-fold change in AUC depending on the historic dataset used for comparison. CsA increased midazolam AUC after oral administration by 1.46-fold compared to different cohorts of stable transplant patients but on matched co-medication (64). Combining the proposed CsA PBPK model and the PBPK model for midazolam (22) allowed simulations of a DDI following an oral dose of Neoral® (380 mg) and an oral solution of midazolam (3 mg). Predicted increase in AUC of 30% was in agreement with the reported clinical data (64) and was mainly driven by the reduction in pre-systemic intestinal metabolism (F_G control and inhibited F_G' were 0.57 and 0.75, respectively). It is noteworthy that the i.v. and oral clearance values of midazolam were considerably different in transplant patients from those of a typical healthy individual, indicating caution in the interpretation of the magnitude of CsA DDIs depending on whether historic data are based on healthy subjects or transplant patients that are likely to be on a number of additional co-medication.

It can be speculated that the large interactions observed *in vivo* between atorvastatin/lovastatin/simvastatin and CsA are caused at least in part by inhibition of intestinal metabolism, considering that the high intestinal extraction of these drugs (42,48) make their oral concentration-time profiles and AUCs more sensitive to inhibition of intestinal CYP3A4 than midazolam or repaglinide. The large interaction potential of CsA in enterocytes is currently based on the assumption that drug concentration within the enterocytes is unbound. Consequently, if this assumption is proven to be incorrect, the interaction potential in the intestine may be reduced.

The prediction of the interaction between CsA and repaglinide was successful using the IC_{50} data against OATP1B1 and OATP1B3 reported here in conjunction with literature data on CYP3A4 inhibitory potency of CsA for repaglinide (58). It is of interest to point out that no change in terminal half-life of repaglinide between control and inhibitory phase was observed. This may be explained by two considerations: first, systemic clearance and volume of distribution change to a similar extent and consequently the elimination rate constant is not affected; this would suggest that, in the case of repaglinide, tissues in addition to liver display permeability/transporter rate limited distribution characteristics which are affected by CsA as the effect on the liver alone would not justify such a change in V_{SS}. Alternatively, the effect of CsA itself has a short duration and the changes in repaglinide pharmacokinetics are predominantly mediated by changes in the first pass effect. The latter explanation fits well with the current assessment that the duration of reduction in transporter activity is relatively short. However, the latter is based on the assumption of reversible inhibition of transporters investigated; it would be of interest to see if the simulations provided in Fig. 8B translate to the *in vivo* situation. Further *in vitro* and *in vivo* data are required to ascertain the true mechanism of cyclosporine inhibition of OATP1B1 and OATP1B3.

Finally, the PK properties of the victim drug are of equal importance as the time course and potency of the inhibitor. While widely accepted in metabolic DDI predictions, this has been mostly ignored in the predictions of transporter-mediated DDIs. As the substrate specificity of uptake transporters is relatively broad and CsA is clearly a potent inhibitor of various processes (in particular of hepatic uptake and intestinal secretion and metabolism), approaches to quantify these DDIs need to be mechanistic and require extensive *in vitro* kinetic data. Consideration of the victim drug properties, such as intracellular binding, metabolism, contribution of passive diffusion, f_T and other properties (intestinal secretion or enterohepatic recirculation), may influence the magnitude of DDI and are problematic to assess using conventional methodologies. We have provided a framework for future assessment of these complex DDIs by developing a mechanistic PBPK model for CsA, one of the most prevalent mediators of these types of interactions.

In conclusion, systemic CsA concentration-time profiles are predictable using PBPK modeling. It is apparent from the CsA potency and predicted local exposure that inhibition of hepatic uptake transporters is of considerably greater DDI importance than inhibition of hepatic metabolism/excretion. In contrast, simulations have illustrated that intestinal efflux transporters and CYP3A are subject to considerable reduction in their activity given the high CsA enterocytic concentrations. The current study provides the mechanistic framework for quantitative prediction of transporter-enzyme mediated DDIs, emphasizing the need to consider the inhibitor concentration at the relevant sites of interaction in conjunction with PK properties of the

victim drug. The combination of victim drug and inhibitor PBPK models should be considered as the state-of-the-art approach for predicting complex DDIs such as those mediated by CsA.

ACKNOWLEDGMENTS AND DISCLOSURES

The authors would like to thank Prof. Leon Aarons and Drs Kayode Ogungbenro and Henry Pertinez for useful discussions and critical review of this article prior to submission. Further, the valuable discussions with Carolina Säll regarding the repaglinide PBPK model are acknowledged.

REFERENCES

1. Hinton LK, Galetin A, Houston JB. Multiple inhibition mechanisms and prediction of drug-drug interactions: status of metabolism and transporter models as exemplified by gemfibrozil-drug interactions. Pharm Res. 2008;25(5):1063–74.
2. Karlgren M, Ahlin G, Bergstrom CA, Svensson R, Palm J, Artursson P. In vitro and in silico strategies to identify OATP1B1 inhibitors and predict clinical drug-drug interactions. Pharm Res. 2012;29(2):411–26.
3. Giacomini KM, Huang SM, Tweedie DJ, Benet LZ, Brouwer KL, Chu X, *et al.* Membrane transporters in drug development. Nat Rev Drug Discov. 2010;9(3):215–36.
4. Yoshida K, Maeda K, Sugiyama Y. Transporter-Mediated Drug-Drug Interactions Involving OATP Substrates: Predictions Based on In Vitro Inhibition Studies. Clin Pharmacol Ther. 2012.
5. Ho RH, Tirona RG, Leake BF, Glaeser H, Lee W, Lemke CJ, *et al.* Drug and bile acid transporters in rosuvastatin hepatic uptake: function, expression, and pharmacogenetics. Gastroenterology. 2006;130(6):1793–806.
6. Kitamura S, Maeda K, Wang Y, Sugiyama Y. Involvement of multiple transporters in the hepatobiliary transport of rosuvastatin. Drug Metab Dispos. 2008;36(10):2014–23.
7. Li J, Volpe DA, Wang Y, Zhang W, Bode C, Owen A, *et al.* Use of transporter knockdown Caco-2 cells to investigate the in vitro efflux of statin drugs. Drug Metab Dispos. 2011;39(7):1196–202.
8. Kahan BD, Shaw LM, Holt D, Grevel J, Johnston A. Consensus document: Hawk's Cay meeting on therapeutic drug monitoring of cyclosporine. Clin Chem. 1990;36(8 Pt 1):1510–6.
9. Aweeka FT, Tomlanovich SJ, Prueksaritanont T, Gupta SK, Benet LZ. Pharmacokinetics of orally and intravenously administered cyclosporine in pre-kidney transplant patients. J Clin Pharmacol. 1994;34(1):60–7.
10. Bauer S, Stormer E, Johne A, Kruger H, Budde K, Neumayer HH, *et al.* Alterations in cyclosporin A pharmacokinetics and metabolism during treatment with St John's wort in renal transplant patients. Br J Clin Pharmacol. 2003;55(2):203–11.
11. Ku YM, Min DI, Flanigan M. Effect of grapefruit juice on the pharmacokinetics of microemulsion cyclosporine and its metabolite in healthy volunteers: does the formulation difference matter? J Clin Pharmacol. 1998;38(10):959–65.
12. Wang CP, Burckart GJ, Ptachcinski RJ, Venkataramanan R, Schwinghammer T, Hakala T, *et al.* Cyclosporine metabolite concentrations in the blood of liver, heart, kidney, and bone marrow transplant patients. Transplant Proc. 1988;20(2 Suppl 2):591–6.
13. Karamperis N, Koefoed-Nielsen PB, Brahe P, Hojskov C, Egfjord M, Poulsen JH, *et al.* Correlations between calcineurin phosphatase inhibition and cyclosporine metabolites concentrations in kidney transplant recipients: implications for immunoassays. Basic Clin Pharmacol Toxicol. 2006;98(6):569–74.
14. Awni WM, Kasiske BL, Heim-Duthoy K, Rao KV. Long-term cyclosporine pharmacokinetic changes in renal transplant recipients: effects of binding and metabolism. Clin Pharmacol Ther. 1989;45(1):41–8.
15. Schwinghammer TL, Przepiorka D, Venkataramanan R, Wang CP, Burckart GJ, Rosenfeld CS, *et al.* The kinetics of cyclosporine and its metabolites in bone marrow transplant patients. Br J Clin Pharmacol. 1991;32(3):323–8.
16. FDA. Guidance for Industry: Drug Interaction Studies—Study Design, Data Analysis, Implications for Dosing, and Labeling Recommendations. http://wwwfdagov/downloads/Drugs/GuidanceComplianceRegulatoryInformation/Guidances/UCM292362pdf. 2012.
17. Amundsen R, Christensen H, Zabihyan B, Asberg A. Cyclosporine A, but not tacrolimus, shows relevant inhibition of organic anion-transporting protein 1B1-mediated transport of atorvastatin. Drug Metab Dispos. 2010;38(9):1499–504.
18. Kawai R, Lemaire M, Steimer JL, Bruelisauer A, Niederberger W, Rowland M. Physiologically based pharmacokinetic study on a cyclosporin derivative, SDZ IMM 125. J Pharmacokinet Biopharm. 1994;22(5):327–65.
19. Kawai R, Mathew D, Tanaka C, Rowland M. Physiologically based pharmacokinetics of cyclosporine A: extension to tissue distribution kinetics in rats and scale-up to human. J Pharmacol Exp Ther. 1998;287(2):457–68.
20. Tanaka C, Kawai R, Rowland M. Physiologically based pharmacokinetics of cyclosporine A: reevaluation of dose-nonlinear kinetics in rats. J Pharmacokinet Biopharm. 1999;27(6):597–623.
21. Bernareggi A, Rowland M. Physiologic modeling of cyclosporin kinetics in rat and man. J Pharmacokinet Biopharm. 1991;19(1):21–50.
22. Gertz M, Houston JB, Galetin A. Physiologically based pharmacokinetic modeling of intestinal first-pass metabolism of CYP3A substrates with high intestinal extraction. Drug Metab Dispos. 2011;39(9):1633–42.
23. Yu LX, Amidon GL. A compartmental absorption and transit model for estimating oral drug absorption. Int J Pharm. 1999;186(2):119–25.
24. Menochet K, Kenworthy KE, Houston JB, Galetin A. Use of mechanistic modelling to assess inter-individual variability and inter-species differences in active uptake in human and rat hepatocytes. Drug Metab Dispos. 2012;40(9):1744-56.
25. Sall C, Houston JB, Galetin A. A comprehensive assessment of repaglinide metabolic pathways: impact of choice of in vitro system and relative enzyme contribution to in vitro clearance. Drug Metab Dispos. 2012;40:1279–89.
26. Shitara Y, Itoh T, Sato H, Li AP, Sugiyama Y. Inhibition of transporter-mediated hepatic uptake as a mechanism for drug-drug interaction between cerivastatin and cyclosporin A. J Pharmacol Exp Ther. 2003;304(2):610–6.
27. Treiber A, Schneiter R, Delahaye S, Clozel M. Inhibition of organic anion transporting polypeptide-mediated hepatic uptake is the major determinant in the pharmacokinetic interaction between bosentan and cyclosporin A in the rat. J Pharmacol Exp Ther. 2004;308(3):1121–9.
28. Campbell SD, de Morais SM, Xu JJ. Inhibition of human organic anion transporting polypeptide OATP 1B1 as a mechanism of drug-induced hyperbilirubinemia. Chem Biol Interact. 2004;150(2):179–87.
29. Ismailos G, Reppas C, Dressman JB, Macheras P. Unusual solubility behaviour of cyclosporin A in aqueous media. J Pharm Pharmacol. 1991;43(4):287–9.

30. Mithani SD, Bakatselou V, TenHoor CN, Dressman JB. Estimation of the increase in solubility of drugs as a function of bile salt concentration. Pharm Res. 1996;13(1):163–7.
31. Legg B, Rowland M. Cyclosporin: erythrocyte binding and an examination of its use to estimate unbound concentration. Ther Drug Monit. 1988;10(1):16–9.
32. Legg B, Gupta SK, Rowland M, Johnson RW, Solomon LR. Cyclosporin: pharmacokinetics and detailed studies of plasma and erythrocyte binding during intravenous and oral administration. Eur J Clin Pharmacol. 1988;34(5):451–60.
33. Kees F, Bucher M, Schweda F, Gschaidmeier H, Burhenne J, Mikus G, *et al.* Comparative bioavailability of the microemulsion formulation of cyclosporine (Neoral) with a generic dispersion formulation (Cicloral) in young healthy male volunteers. Ther Drug Monit. 2006;28(3):312–20.
34. Venkataramanan R, Starzl TE, Yang S, Burckart GJ, Ptachcinski RJ, Shaw BW, *et al.* Biliary Excretion of Cyclosporine in Liver Transplant Patients. Transplant Proc. 1985;17(1):286–9.
35. Ducharme MP, Warbasse LH, Edwards DJ. Disposition of intravenous and oral cyclosporine after administration with grapefruit juice. Clin Pharmacol Ther. 1995;57(5):485–91.
36. Gupta SK, Manfro RC, Tomlanovich SJ, Gambertoglio JG, Garovoy MR, Benet LZ. Effect of food on the pharmacokinetics of cyclosporine in healthy subjects following oral and intravenous administration. J Clin Pharmacol. 1990;30(7):643–53.
37. Tsang VT, Johnston A, Heritier F, Leaver N, Hodson ME, Yacoub M. Cyclosporin pharmacokinetics in heart-lung transplant recipients with cystic fibrosis. Effects of pancreatic enzymes and ranitidine. Eur J Clin Pharmacol. 1994;46(3):261–5.
38. Min DI, Lee M, Ku YM, Flanigan M. Gender-dependent racial difference in disposition of cyclosporine among healthy African American and white volunteers. Clin Pharmacol Ther. 2000;68(5):478–86.
39. Lehle K, Kirchner GI, Rupprecht L, Gruber M, Birnbaum DE, Schmid FX, *et al.* A prospective cross-over study comparing the pharmacokinetics of cyclosporine A and its metabolites after oral versus short-time intravenous cyclosporine A administration in pre-heart transplant patients. Transplant Proc. 2007;39(10):3323–8.
40. Steimer W. Performance and specificity of monoclonal immunoassays for cyclosporine monitoring: how specific is specific? Clin Chem. 1999;45(3):371–81.
41. Rostami-Hodjegan A, Tucker GT. The effects of portal shunts on intestinal cytochrome P450 3A activity. Hepatology (Baltimore, Md). 2002;35(5):1549–50.
42. Gertz M, Harrison A, Houston JB, Galetin A. Prediction of human intestinal first-pass metabolism of 25 CYP3A substrates from in vitro clearance and permeability data. Drug Metab Dispos. 2010;38(7):1147–58.
43. Chiu YY, Higaki K, Neudeck BL, Barnett JL, Welage LS, Amidon GL. Human jejunal permeability of cyclosporin A: influence of surfactants on P-glycoprotein efflux in Caco-2 cells. Pharm Res. 2003;20(5):749–56.
44. Drewe J, Beglinger C, Kissel T. The absorption site of cyclosporin in the human gastrointestinal tract. Br J Clin Pharmacol. 1992;33(1):39–43.
45. Hintz RJ, Johnson KC. The effect of particle size distribution on dissolution rate and oral absorption. Int J Pharm. 1989;51(1):9–17.
46. Persson E, Gustafsson A-S, Carlsson A, Nilsson R, Knutson L, Forsell P, *et al.* The effects of food on the dissolution of poorly soluble drugs in human and in model small intestinal fluids. Pharm Res. 2005;22(12):2141–51.
47. Lennernas H. Intestinal permeability and its relevance for absorption and elimination. Xenobiotica; the fate of foreign compounds in biological systems. 2007;37(10–11):1015–51.
48. Gertz M, Davis JD, Harrison A, Houston JB, Galetin A. Grapefruit juice-drug interaction studies as a method to assess the extent of intestinal availability: utility and limitations. Curr Drug Metab. 2008;9(8):785–95.
49. Foti RS, Rock DA, Wienkers LC, Wahlstrom JL. Selection of alternative CYP3A4 probe substrates for clinical drug interaction studies using in vitro data and in vivo simulation. Drug Metab Dispos. 2010;38(6):981–7.
50. Sall C, Gertz M, Menochet K, Houston JB, Galetin A. A physiologically-based pharmacokinetic modelling approach for repaglinide clearance and drug-drug interactions: impact of in vitro system and role of transporter-metabolism interplay. drug metabolism reviews. 2012.
51. Rodgers T, Rowland M. Physiologically based pharmacokinetic modelling 2: predicting the tissue distribution of acids, very weak bases, neutrals and zwitterions. J Pharm Sci. 2006;95(6):1238–57.
52. Ito K, Hallifax D, Obach RS, Houston JB. Impact of parallel pathways of drug elimination and multiple cytochrome P450 involvement on drug-drug interactions: CYP2D6 paradigm. Drug Metab Dispos. 2005;33(6):837–44.
53. Kalliokoski A, Backman JT, Neuvonen PJ, Niemi M. Effects of the SLCO1B1*1B haplotype on the pharmacokinetics and pharmacodynamics of repaglinide and nateglinide. Pharmacogenet Genomics. 2008;18(11):937–42.
54. Kalliokoski A, Neuvonen M, Neuvonen PJ, Niemi M. Different effects of SLCO1B1 polymorphism on the pharmacokinetics and pharmacodynamics of repaglinide and nateglinide. J Clin Pharmacol. 2008;48(3):311–21.
55. Kalliokoski A, Neuvonen M, Neuvonen PJ, Niemi M. The effect of SLCO1B1 polymorphism on repaglinide pharmacokinetics persists over a wide dose range. Br J Clin Pharmacol. 2008;66(6):818–25.
56. Niemi M, Backman JT, Kajosaari LI, Leathart JB, Neuvonen M, Daly AK, *et al.* Polymorphic organic anion transporting polypeptide 1B1 is a major determinant of repaglinide pharmacokinetics. Clin Pharmacol Ther. 2005;77(6):468–78.
57. Paine MF, Khalighi M, Fisher JM, Shen DD, Kunze KL, Marsh CL, *et al.* Characterization of interintestinal and intraintestinal variations in human CYP3A-dependent metabolism. J Pharmacol Exp Ther. 1997;283(3):1552–62.
58. Kajosaari LI, Niemi M, Neuvonen M, Laitila J, Neuvonen PJ, Backman JT. Cyclosporine markedly raises the plasma concentrations of repaglinide. Clin Pharmacol Ther. 2005;78(4):388–99.
59. Noe J, Portmann R, Brun ME, Funk C. Substrate-dependent drug-drug interactions between gemfibrozil, fluvastatin and other organic anion-transporting peptide (OATP) substrates on OATP1B1, OATP2B1, and OATP1B3. Drug Metab Dispos. 2007;35(8):1308–14.
60. Karlgren M, Vildhede A, Norinder U, Wisniewski JR, Kimoto E, Lai Y, *et al.* Classification of inhibitors of hepatic organic anion transporting polypeptides (OATPs): influence of protein expression on drug-drug interactions. J Med Chem. 2012;55(10):4740–63.
61. Tanaka C, Kawai R, Rowland M. Dose-dependent pharmacokinetics of cyclosporin A in rats: events in tissues. Drug Metab Dispos. 2000;28(5):582–9.
62. Kovarik JM, Mueller EA, van Bree JB, Tetzloff W, Kutz K. Reduced inter- and intraindividual variability in cyclosporine pharmacokinetics from a microemulsion formulation. J Pharm Sci. 1994;83(3):444–6.
63. Li G, Treiber G, Meinshausen J, Wolf J, Werringloer J, Klotz U. Is cyclosporin A an inhibitor of drug metabolism? Br J Clin Pharmacol. 1990;30(1):71–7.

64. de Jonge H, de Loor H, Verbeke K, Vanrenterghem Y, Kuypers DR. In vivo CYP3A activity is significantly lower in cyclosporine-treated as compared with tacrolimus-treated renal allograft recipients. Clin Pharmacol Ther. 2011;90(3):414–22.
65. Hedman M, Antikainen M, Holmberg C, Neuvonen M, Eichelbaum M, Kivisto KT, *et al.* Pharmacokinetics and response to pravastatin in paediatric patients with familial hypercholesterolaemia and in paediatric cardiac transplant recipients in relation to polymorphisms of the SLCO1B1 and ABCB1 genes. Br J Clin Pharmacol. 2006;61(6):706–15.
66. Niemi M, Pasanen MK, Neuvonen PJ. SLCO1B1 polymorphism and sex affect the pharmacokinetics of pravastatin but not fluvastatin. Clin Pharmacol Ther. 2006;80(4):356–66.
67. Pasanen MK, Neuvonen M, Neuvonen PJ, Niemi M. SLCO1B1 polymorphism markedly affects the pharmacokinetics of simvastatin acid. Pharmacogenet Genomics. 2006;16(12):873–9.
68. Weber C, Schmitt R, Birnboeck H, Hopfgartner G, Eggers H, Meyer J, *et al.* Multiple-dose pharmacokinetics, safety, and tolerability of bosentan, an endothelin receptor antagonist, in healthy male volunteers. J Clin Pharmacol. 1999;39(7):703–14.